2008

Evaluation of bridges implementing innovative materials and design

Mark Thomas Giesmann
Iowa State University

Evaluation of bridges implementing innovative materials and design

by

Mark Thomas Giesmann

A thesis submitted to the graduate faculty

in partial fulfillment of the requirements for the degree of

MASTER OF SCIENCE

Major: Civil Engineering (Structural Engineering)

Program of Study Committee:
Brent M. Phares, Co-major Professor
Terry J. Wipf, Co-major Professor
Loren W. Zachary

Iowa State University

Ames, Iowa

2008

TABLE OF CONTENTS

LIST OF FIGURES v

LIST OF TABLES vii

ACKNOWLEDGMENTS viii

CHAPTER 1. GENERAL INTRODUCTION 1

1.1. Introduction 1

1.2. Thesis Organization 2

1.3. References 3

CHAPTER 2. DESIGN AND PERFORMANCE OF A SINGLE-SPAN STEEL-GIRDER BRIDGE USING A STEEL-FREE DECK SYSTEM 4

2.1. Abstract 4

2.2. Introduction 4

2.3. Design and Construction 6

2.4. Experimental Test Plan 12

2.5. Load Paths 17

2.6. Test Results 19

2.6.1. Deflections 19

2.6.2. Girder Strains 21

2.6.3. Concrete Deck Principal Strains and Stresses 22

2.6.4. Transverse Steel Strap Strains and Stresses 24

2.6.5. Comparing Transverse Steel Strap Strain with Concrete Deck Strain 25

2.6.6. Distribution Factors 26

2.7. Conclusions 27

2.8. References 29

CHAPTER 3. PERFORMANCE EVALUATION OF A SINGLE-SPAN ULTRA-HIGH PERFORMANCE CONCRETE GIRDER BRIDGE 31

3.1. Abstract 31

3.2. Introduction 31

3.3. Design and Construction 33

3.4. Large-Scale Laboratory Flexure Testing 37

3.4.1. Test Specimen 37

3.4.2. Flexural Testing Configuration 37

3.4.3. Test Procedure 38

3.5. Large-Scale Laboratory Flexure Test Results 39

3.6. Live Load Testing 42

3.6.1. Test Configuration 43

3.6.2. Test Procedure 45

3.6.2.1. Pseudo-Static Loading 45

3.6.2.1. Dynamic Loading 45

3.7. Live Load Test Results 47

3.7.1. Bottom Flange Midspan Girder Strains 47

3.7.2. Neutral Axis 49

3.7.3. Load Fraction 51

3.7.4. Distribution Factors 52

3.7.5. Dynamic Results 53

3.8. Comparative Results 56

3.8.1. Bottom Flange Midspan Girder Strain Comparisons 56

3.8.2. Comparison of Live Load Tests and Laboratory Tests 57

3.9. Conclusions 58

3.10. References 60

CHAPTER 4. GENERAL CONCLUSION 61

LIST OF FIGURES

Figure 2.1. Cross section of a typical SFD [adapted from Ventura, 1998]. 6
Figure 2.2. Plan view of the deck system used in the SFD bridge. 11
Figure 2.3. Slab details in the TCB bridge. 11
Figure 2.4. Epoxy coated steel and GFRP reinforcement. 12
Figure 2.5. Elevation of Tama County SFD bridge. 12
Figure 2.6. Instrumentation plan for Test 1. 14
Figure 2.7. Instrumentation plan for Test 2. 15
Figure 2.7. Continued. 16
Figure 2.8. Placement of strain transducer rosettes for Test 2 looking towards midspan. 16
Figure 2.9. Test vehicles' configurations and axle loads. 17
Figure 2.10. Load Case 1 (stationary) during Test 1. 18
Figure 2.11. Load cases used in Test 1 and Test 2. 18
Figure 2.12. Maximum girder deflections at midspan from Test 1 and Test 2. 20
Figure 2.13. Maximum girder strains at midspan from Test 1 and Test 2. 21
Figure 2.14. Transverse steel strap strain and concrete deck strain (Load Case 6) located between Girders 3 and 4 at midspan from Test 2. 25
Figure 2.15. Experimental and AASHTO Distribution Factors from Test 1 and Test 2. 27
Figure 3.1. Cross section of Wapello County UHPC bridge. 35
Figure 3.2. Cross sections of Wapello County UHPC bridge beams. 35
Figure 3.3. Elevation of Wapello County UHPC bridge beams. 36
Figure 3.4. Elevation of Wapello County UHPC bridge. 36
Figure 3.5. Large-scale flexure test setup diagram. 38
Figure 3.6. Flexural cracks on bottom flange at midspan during large-scale flexure test. 39
Figure 3.7. Strain at midspan during large-scale flexure test. 41
Figure 3.8. Deflection at midspan during large-scale flexure test. 41
Figure 3.9. Longitudinal live load stresses at cracking of large-scale flexure test beam. 42
Figure 3.10. Strand slip during large-scale flexure test. 42
Figure 3.11. BDI strain transducers attached to concrete. 43

Figure 3.12. Location of BDI strain transducers used during both tests. 44
Figure 3.13. Test vehicle configuration..... 46
Figure 3.14. Truck positions used in the live load tests. 47
Figure 3.15. Maximum bottom flange girder strains at midspan for Test 1..... 49
Figure 3.16. Maximum bottom flange girder strains at midspan for Test 2..... 49
Figure 3.17. Experimental load fractions from Test 1. 51
Figure 3.18. Experimental load fractions from Test 2. 52
Figure 3.19. Experimental and AASHTO distribution factors from Test 1 and Test 2. 53
Figure 3.20. Bottom flange midspan girder strain versus time, Load Case 7, Test 1..... 54
Figure 3.21. Bottom flange girder strains at midspan from Test 1 and Test 2. 56

LIST OF TABLES

Table 2.1. Bridge overhang steel reinforcement details. 11
Table 2.2. Summary of test vehicles' configuration and axle loads. 17
Table 3.1. Typical UHPC material composition [2]. 33
Table 3.2. Comparison of large-scale flexure test capacities to applied bridge moments. 41
Table 3.3. Summary of test vehicle's configurations and weights. 46
Table 3.4. Neutral axis location measured from the bottom flange. 50

ACKNOWLEDGMENTS

First, I would like to thank my parents and family for their support and encouragement throughout my life. I would like to especially thank my wife, Amanda, for her patience, understanding, and encouragement during my study. This thesis would not have been possible without their love and source of strength.

I would like to express my appreciation to my major professors, Dr. Terry J. Wipf and Dr. Brent M. Phares, for their guidance, advice, and assistance. I would also like to thank Dr. Loren W. Zachary for serving on my committee. Special thanks to Douglas L. Wood, Structural Engineering Laboratory Manager, who provided significant assistance with the field testing. Gratitude is also extended to my fellow civil engineering graduate students and the professors, staff, and faculty at the Center for Transportation Research and Education and the Civil, Construction and Environmental Engineering Department at Iowa State University.

The research projects presented in this thesis were initiated by the Iowa Department of Transportation and sponsored by the Federal Highway Administration. In addition, thanks are expressed to Lyle Brehm (Tama County Engineer) and Brian Moore (Wapello County Engineer) for their help in various phases of these projects.

CHAPTER 1. GENERAL INTRODUCTION

1.1. INTRODUCTION

According to the Federal Highway Administration (FHWA) and the 2007 National Bridge Inventory [1], approximately 25% of the United States' 600,000 bridges are considered structurally deficient or functionally obsolete. In the state of Iowa, nearly 27% of the state's 25,000 bridges are similarly classified and in need of repair or replacement. As these bridges deteriorate, expensive rehabilitations and replacements are required while budgets are limited. In 1998, the FHWA created the Innovative Bridge Research and Construction (IBRC) Program aimed to demonstrate and provide funding for repair, rehabilitation, replacement, and new construction of bridges using innovative materials [2]. The objective of the program is to develop new, cost effective, innovative materials that will reduce the maintenance cost and overall life cycle cost of the bridge. Further intentions of the program are to develop innovative bridge designs that result in shallower superstructures, longer spans, and utilization of high performance materials. Additional funding is available for performance evaluation and performance monitoring of the bridge following construction.

Partially funded through the IBRC Program, the two projects summarized in this thesis demonstrate the use of innovative concepts and materials for bridge applications. The projects presented in this thesis concentrate on the validation and performance evaluation of two bridges that implement newly developed materials and design.

1.2. THESIS ORGANIZATION

This thesis contains two separate papers related to the performance evaluation and demonstration of two bridges in the state of Iowa that make use of innovative materials and bridge design. Live load field tests were completed between the fall of 2005 and the summer of 2007. Both projects were funded in part by the FHWA through the IBRC Program.

The first paper highlights the design and performance evaluation of a bridge deck replacement in Tama County, Iowa that makes use of a new system in which there is no internal reinforcing steel within the concrete deck. The paper was written for submittal in the *Journal of Bridge Engineering*. The thesis author is the primary author of this paper. Van W. Robbins performed research on the design and construction of the project as a graduate student at Iowa State University (ISU) and Mark J. Dunn performed the first live load field test as a graduate student at ISU. The remaining authors listed are professors at ISU and provided guidance and assistance throughout the project.

The second paper highlights the design and evaluation of bridge constructed in Wapello County, Iowa that utilizes a newly developed material referred to as Ultra-High Performance Concrete. The second paper was written for submittal in the *Journal of Bridge Engineering*. The thesis author is the primary author of this paper. Brian E. Degen performed research on the design, construction, and laboratory testing of the project as a graduate student at ISU. The other authors listed are professors at ISU and provided guidance and assistance throughout the completion of the project.

1.3. REFERENCES

1. Federal Highway Administration, National Bridge Inventory, NBI Report, 2007. http://www.fhwa.dot.gov/bridge/deficient.htm
2. Federal Highway Administration, Innovative Bridge Research and Construction (IBRC) Program, 2006. http://www.fhwa.dot.gov/bridge/ibrc/

CHAPTER 2. DESIGN AND PERFORMANCE OF A SINGLE-SPAN STEEL-GIRDER BRIDGE USING A STEEL-FREE DECK SYSTEM

A paper to be submitted to the *Journal of Bridge Engineering*

Mark T. Giesmann, Van W. Robbins, Mark J. Dunn,

Terry J. Wipf, Brent M. Phares, F. Wayne Klaiber

2.1. ABSTRACT

Concrete bridge decks exposed to harsh temperatures and a variety of deicing chemicals are suspect to deterioration caused by corrosion of the steel reinforcement. By removing the steel reinforcement within the concrete slab, the life expectancy and durability of the bridge deck can be expected to improve greatly [1]. Researchers at the Bridge Engineering Center at Iowa State University have researched, designed, and tested the first known bridge in the United States that has implemented a steel-free deck (SFD) system. The bridge deck consists of a fiber reinforced deck with no internal reinforcing steel that is composite with the steel superstructure. Transverse steel straps below the slab are attached to the supporting girders to prevent outward lateral displacement and to develop internal arching action within the concrete. This paper describes the design and construction of the SFD bridge, and then presents the results of live load field tests conducted on the completed bridge.

2.2. INTRODUCTION

Corrosion of the reinforcing steel in bridge decks causes a substantial decrease in durability and life expectancy. As cracks in the concrete open, reinforcing bars are exposed

to air and moisture, which initiates corrosion of the steel. In addition, North America's dramatic temperature fluctuations and heavy use of deicing salts further exacerbates the steel corrosion. The expansive corrosion of the reinforcement causes additional cracking, spalling, and deterioration of the concrete deck requiring costly repairs and reducing the life expectancy of the bridge. Protecting or eliminating the steel reinforcement from corrosive agents minimizes this effect [1]. The Bridge Engineering Center (BEC) at Iowa State University (ISU) recently researched, designed, and evaluated the use of a steel-free deck (SFD) system.

A bridge employing the SFD system was designed, tested, and constructed by the Ministry of Transportation of Ontario. No internal steel reinforcement was used in the deck of the bridge. Instead, external steel straps were attached to the top flange of the supporting girders to prohibit outward lateral displacement. As a result of the transverse confinement, compressive internal arching action is promoted within the concrete in which the steel strap carries the horizontal tension force. Figure 2.1 depicts a typical SFD system cross section. The internal arching action encourages a punching shear behavior that produces an increased load capacity when compared to flexural behavior [2]. Technical documentation of this type of SFD predicts load carrying capacities of more than four times the capacity required by the Ontario Highway Bridge Design Code (OHBDC) [3, 4]. The Canadian Highway Bridge Design Code (CHBDC) [5], which replaced the OHBDC in December of 2000, now includes design guidelines for a SFD system.

This paper presents a performance evaluation of the first know SFD bridge built in the United States which is located in Tama County, Iowa. The Tama County Bridge (TCB) was instrumented at critical locations to monitor the bridge behavior during two separate field

load tests. Background, design, and construction of the TCB are presented here; however, the focus of this paper is to present the results of the load tests.

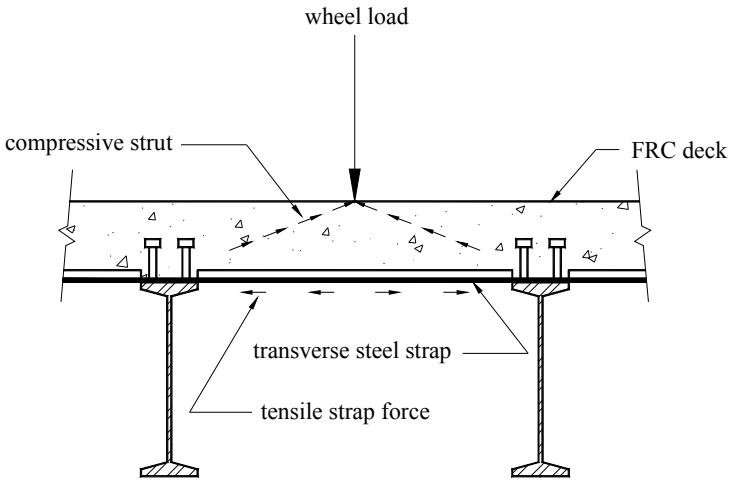

Figure 2.1. Cross section of a typical SFD [adapted from Ventura, 1998].

2.3. DESIGN AND CONSTRUCTION

The original TCB was constructed in 1941 and the first deck was replaced in 1961. Consisting of seven steel girders spaced 3 ft – 8 in. on center, the original bridge spanned 41 ft and had a 24 ft wide roadway. In the summer of 2004, the deck was replaced by the SFD system and the roadway was widen to 28 ft by extending the exterior girder spacing to 5 ft and increasing the overhang to 1 ft – 6½ in.

Researchers in the BEC at ISU designed the section of the deck slab between the centerlines of the exterior girders using the SFD system guidelines and design requirements provided by the CHBDC. In the absence of steel reinforcement, a composite fiber reinforced concrete (FRC) deck, instead of traditional concrete, was used along with glass fiber reinforced polymer (GRFP) bars to control temperature and shrinkage effects. Since FRC is

not a common material used in Iowa, a Special Provision to the Iowa Department of Transportation (Iowa DOT) Standard Specifications for Construction [7] was drafted for its use in the SFD. The slab overhang was designed using conventional reinforced concrete design practices provided by the 1996 American Association of State Highway Transportation Officials Standard Specifications for State Highway Bridges, Sixteenth Edition (AASHTO) [6].

The following is a list of requirements specified by the CHBDC for a SFD as well as information on how the TCB either satisfied or was modified to meet these requirements (Note that the following dimensions and equations have been converted from metric units given in the CHBDC to English units):

1. A SFD that meets the specified requirements only needs to be structurally analyzed in negative moment regions such as the deck overhang. However, since the TCB is a single span bridge with a conventional reinforced concrete overhang, these requirements are not discussed here.
2. The deck is to act compositely with parallel supporting girders in positive moment regions. As such, shear stud connectors were added to the top flange of the existing steel girders.
3. The girder spacing "S" cannot be more than 9 ft – 10 in. As previously stated, the maximum girder spacing in the TCB is 5 ft.
4. The minimum allowable deck thickness is the maximum of either 7 in. or S/15. For the TCB, the girder spacing does not control and a conservative 8.5 in. deck was used.
5. The required haunch height must be between 1 in. and 5 in. to provide clearance between the transverse steel strap and FRC deck. A nominal haunch height of 1.5 in.

was used for the TCB.

6. Shear stud connectors are required to project into the FRC slab a minimum of 3 in. and have a top clearance of at least 4 in. if deicing salts are used or 3 in. otherwise. Deicing salts will be applied to the TCB during the winter months therefore a 4 in. shear stud top clearance was used. Based on the above requirements, a nominal shear stud length of 6 in. was used with a diameter of 0.875 in. installed in pairs at a spacing of 16 in. on center.
7. The transverse free edge of the FRC deck (e.g., the simply supported end of the bridge) must have a minimum flexural rigidity of:

$$EI = 22.3\left(L_U\right)^4 \qquad (2.1)$$

Where:

EI = flexural rigidity (kip-ft^2).

L_U = transverse free edge length (i.e., flange tip to flange tip in ft).

If L_U is less than 13 ft – 11 in., this requirement can be satisfied if the details specified in the CHBDC are used. The ends of the girders on the TCB are fully encased in concrete to act as a retaining structure for the soil behind the bridge abutment. In this case, the transverse free edge of slab is bearing directly on the abutment pile cap and is not subjected to bending loads.

8. The maximum transverse diaphragm spacing is 26 ft – 2 in. In the TCB, a transverse diaphragm is located at midspan, 21 ft from the centerline of bearing of both abutments as shown in Figure 2.2.
9. The minimum required transverse steel strap area is determined with Equation 2.2:

$$A = \frac{F_S (S)^2 S_1}{Et} 250.56 \quad (2.2)$$

Where:

A = cross sectional area of the transverse steel strap (in.^{2}).

F_S = 5.0 for interior girders bays and 6.0 for exterior girder bays.

S = girder spacing (ft).

S_1 = transverse steel strap spacing (ft).

E = Young's Modulus (ksi).

t = deck thickness (in.).

In the TCB, a 0.5 x 2-in. steel strap was selected and the resulting area was used to determine the required strap spacing, S_1. The exterior girder bay, which has the largest girder spacing, produced the smallest required transverse steel strap spacing of 6.56 ft. However, this spacing was greater than the maximum allowable spacing of 4.1 ft specified by the CHBDC. Therefore, a transverse steel strap spacing of 4 ft was used.

10. The direct or indirect connection of the transverse steel strap to supporting girders must have a strength (in kips) equal to, or greater than, the steel strap cross sectional area (in in.^{2}) multiplied by 29. The transverse steel straps which are welded to the top flange of the supporting girders of the TCB required a connection shear strength of at least 29.0 kips. The weld was designed using the American Institute of Steel Construction, Load and Resistance Factor Design [8]. The transverse steel straps are continuous over supporting girders; therefore half of the design connection strength for each girder flange was designated to each adjacent girder bay.

11. A sufficient fiber volume fraction is required in the FRC deck to provide a residual strength index of at least 0.30. The residual strength index is the average ratio of post-crack strength to first crack strength determined by testing at least five test beams. On the recommendation of the Iowa DOT, Office of Materials, it was decided to use a structural polymer fiber with a dosage rate that will provide an equivalent flexural strength of at least 250 psi. The projected dosage rate was between 6 lbs and 10 lbs per cubic yard of concrete; an actual fiber dosage rate of 9.2 lbs per cubic yard of concrete was used in the TCB.

The only internal reinforcement between the exterior girders (positive moment region) is a GFRP grid of .375 in. diameter bars in the longitudinal direction spaced at 16 in. on centers and spaced at 10 in. on centers in the transverse direction. The GFRP grid was used to prevent unsightly longitudinal flexural cracks on the underside of the FRC deck and to control temperature and shrinkage effects. Details of the bridge are shown in Figures 2.2 and 2.3, and the GRFP grid and overhang reinforcement during construction is shown in Figure 2.4.

The deck overhang was designed using conventional reinforced concrete and epoxy coated steel reinforcement bars using the AASHTO code. Table 2.1 summarizes the reinforcement provided in the overhang region and can also be seen in Figure 2.3. An elevation view of the completed Tama County SFD bridge is shown in Figure 2.5.

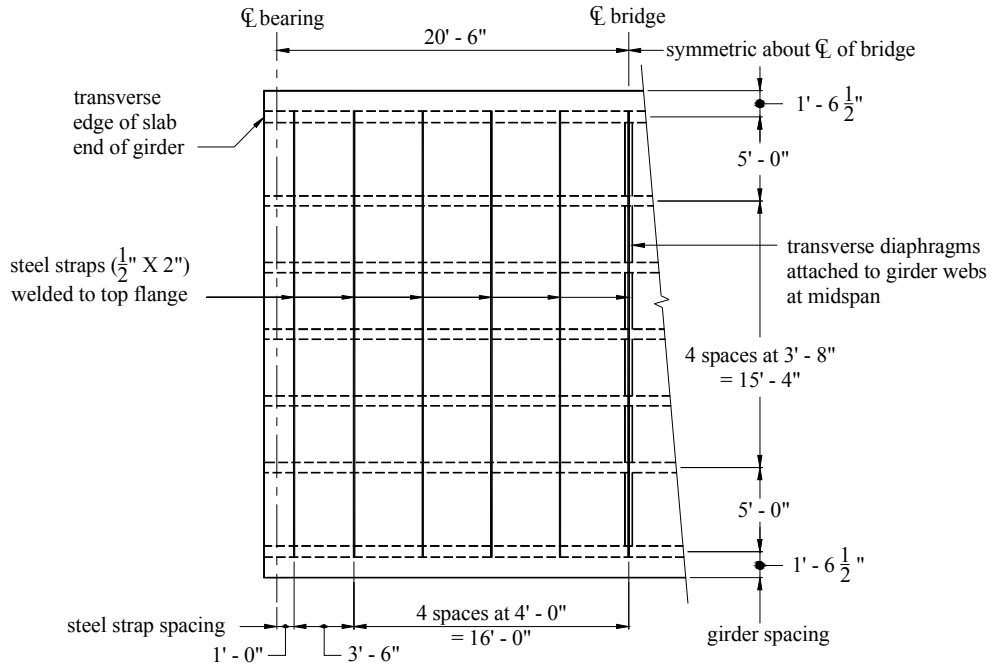

Figure 2.2. Plan view of the deck system used in the SFD bridge.

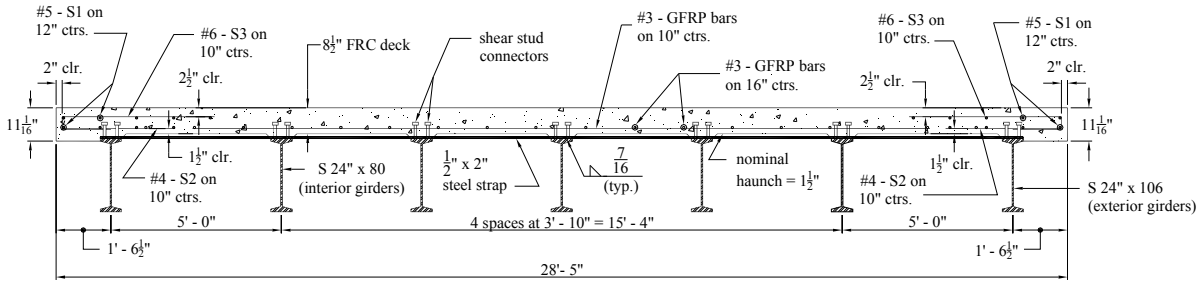

Note: Thrie beam bridge rail not shown.

Figure 2.3. Slab details in the TCB bridge.

Table 2.1. Bridge overhang steel reinforcement details.

Deck Face	Reinforcement direction (relative to flow of traffic)	Bar size (#)	Spacing (in.)	Total bridge quantity
top (S1)	parallel	5	12	10
bottom (S1)	parallel	5	12	8
bottom (S2)	perpendicular	4	10	104
top (S3)	perpendicular	6	10	104

Figure 2.4. Epoxy coated steel and GFRP reinforcement.

Figure 2.5. Elevation of Tama County SFD bridge.

2.4. EXPERIMENTAL TEST PLAN

The initial load test (Test 1), which took place November 16, 2005, was developed with a focus on the general response at midspan and at other local areas of interest. In addition, a specific goal was to examine the correlation between the response of the transverse steel straps and the concrete bridge deck. Girder deflections were recorded using

ratiometric displacement transducers and an Optim Megadac data acquisition system (DAS). Strains were measured using Bridge Diagnostics, Inc. (BDI) Intelliducers and the Structural Testing System (STS). Approximately one year after Test 1, Test 2 was conducted to compare with and to supplement the results from Test 1; Test 2 was conducted on October 5, 2006. The same types of sensors that were used during Test 1 were also used to measure strains and deflections at various points of interest in Test 2.

The instrumentation plan used for Test 1 is shown in Figure 2.6. Seven deflection transducers were attached to the bottom side of each girder at midspan. Eleven strain transducers were placed on the seven girders at midspan (top and bottom flanges of four girders and bottom only on the other three girders) and another 11 strain transducers were placed on transverse steel straps. Fourteen transducers were placed on the underside of the bridge deck to measure the concrete strains. Six of these concrete transducers were placed in groups of three to create two strain rosettes, oriented at 0-45-90 degrees. A total of 36 strain transducers and seven deflection transducers were used on the SFD bridge during Test 1.

Figure 2.7 shows the instrumentation plan used in Test 2. Seven deflection transducers were attached to the bottom side of each girder at midspan. Twelve strain transducers were placed on the seven girders at midspan (top and bottom on five girders and bottom only on two girders) and an additional four strain transducers were attached to the transverse steel straps. Twenty-four transducers were attached to the concrete deck in groups of three to form eight strain rosettes, oriented at 0-45-90 degrees. The purpose for using the rosettes was to determine the location and magnitude of the principal concrete strains. Figure 2.8 shows the placement of the strain rosettes on the bridge deck. A total of 40 strain transducers and seven deflection transducers were used in the instrumentation of Test 2.

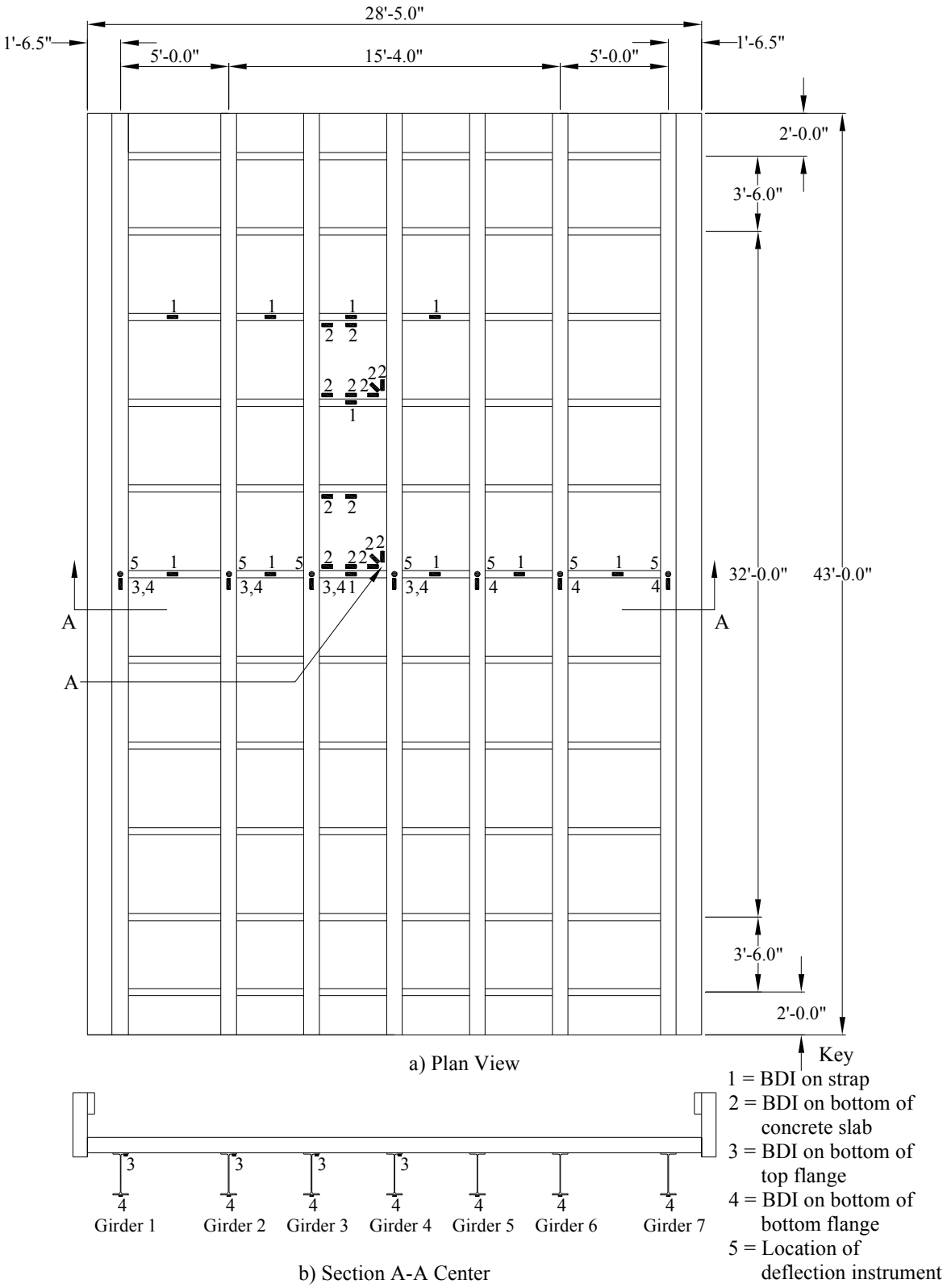

Figure 2.6. Instrumentation plan for Test 1.

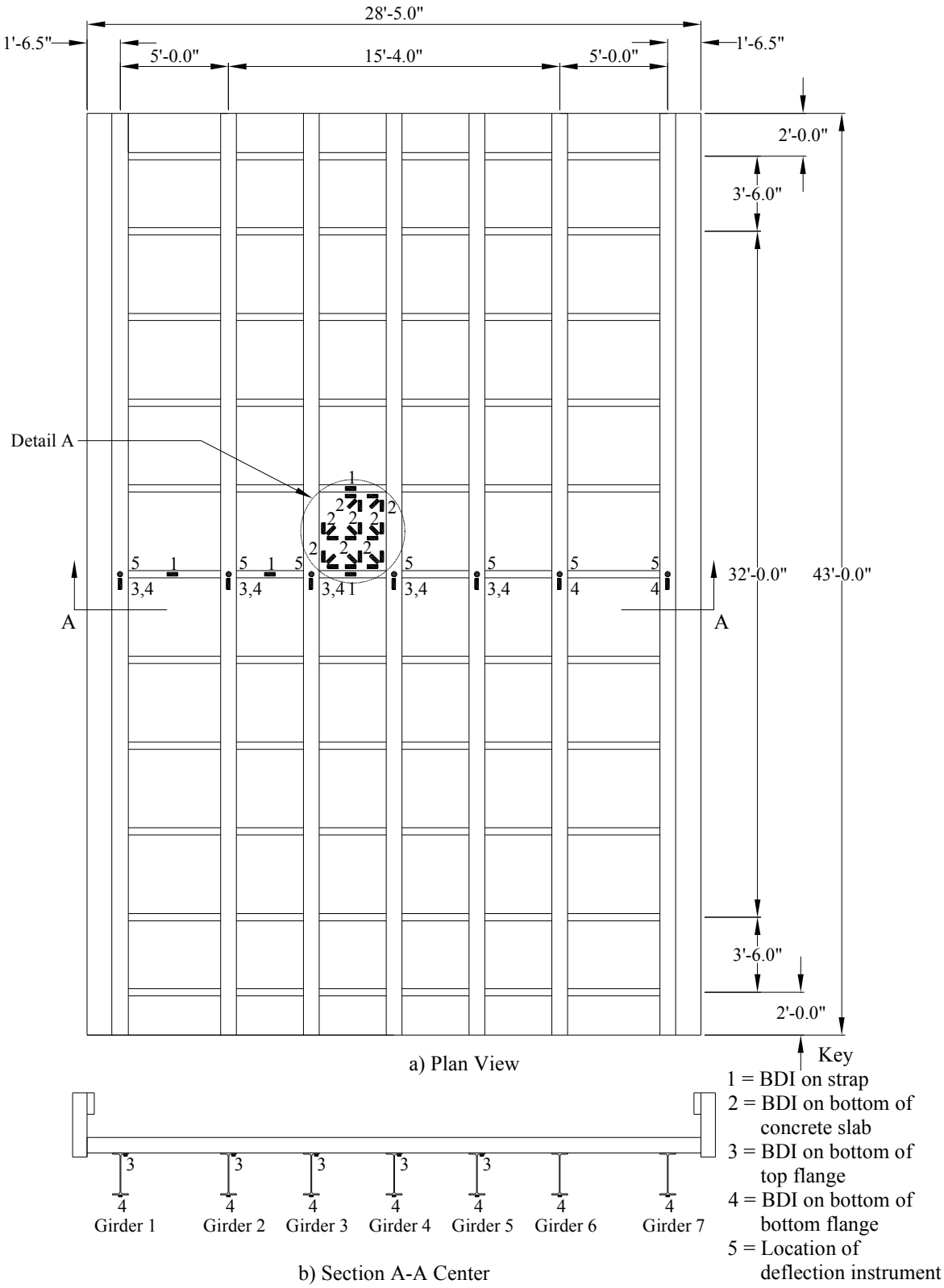

Figure 2.7. Instrumentation plan for Test 2.

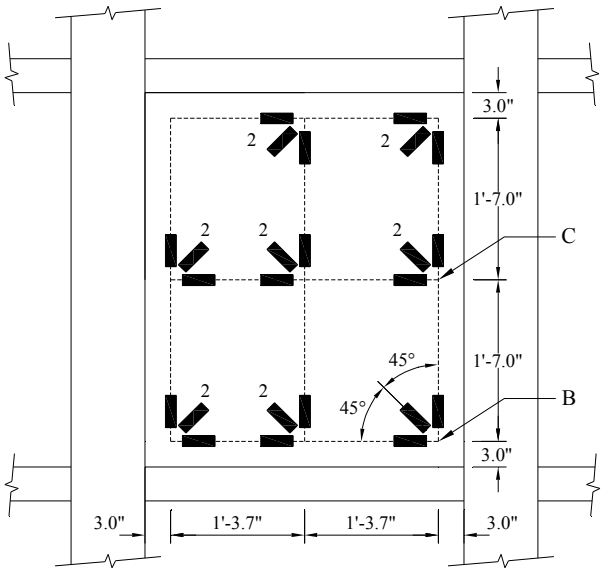

c) Detail A showing strain transducer rosettes.

Figure 2.7. Continued.

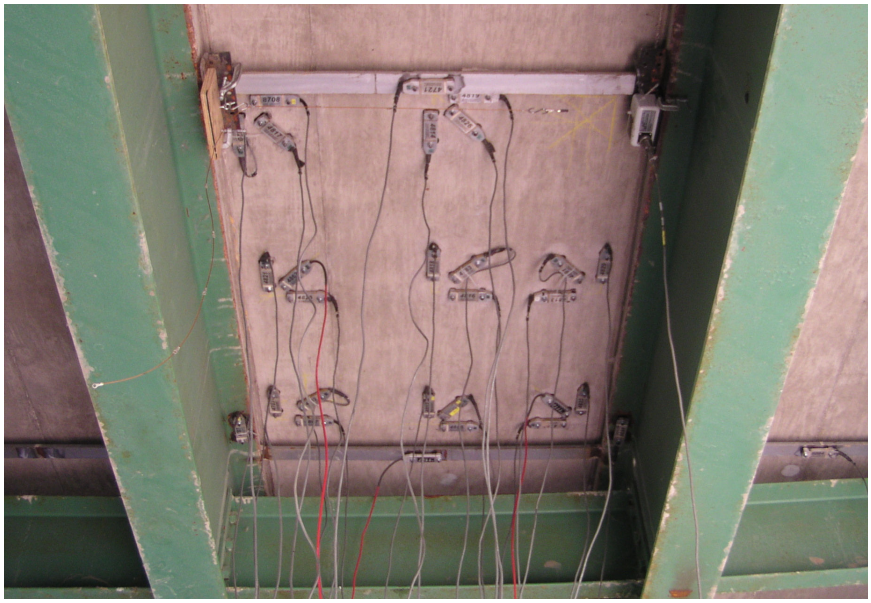

Figure 2.8. Placement of strain transducer rosettes for Test 2 looking towards midspan.

The bridge was loaded in each of the tests using two loaded tandem-axle dump trucks provided by the Tama County Secondary Roads Department. The vehicles' weights and configurations for each test are summarized in Table 2.2 and Figure 2.9.

Table 2.2. Summary of test vehicles' configuration and axle loads.

	Test Vehicle	Front Axle Weight (lbs)	Dimensions 'a'	'b'	'c'	Rear Axles Weight (lbs)	Total Weight (lbs)
Test 1	1	18,940	7'-1"	4'-5"	6'-0"	32,740	51,680
	2	17,680	6'-9"	4'-5"	6'-0"	35,180	52,860
Test 2	1	15,130	7'-1"	4'-6"	6'-1"	35,320	50,450
	2	17,300	6'-9"	4'-6"	6'-1"	35,480	52,780

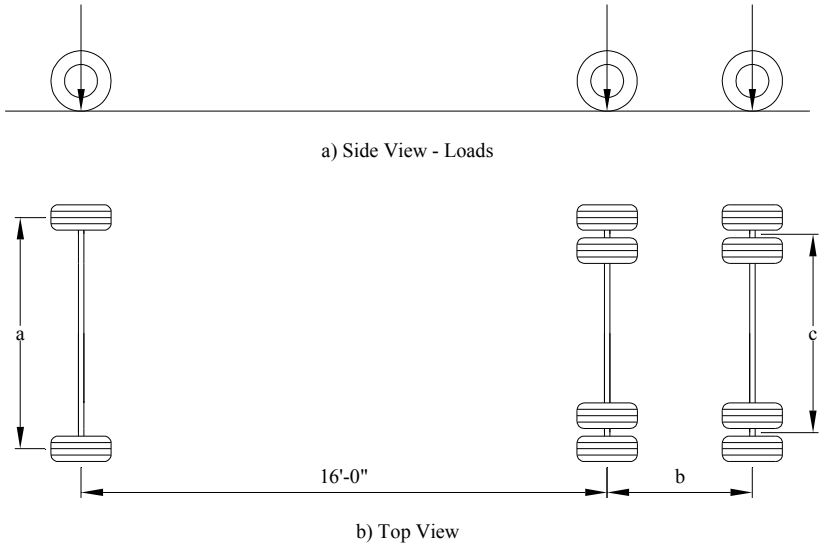

Figure 2.9. Test vehicles' configurations and axle loads.

2.5. LOAD PATHS

Each load test consisted of seven different load cases. Two stationary load tests (Load Cases 1 and 2) were conducted each once with both trucks on the bridge with the tandem axles at midspan as shown in Figure 2.10. Five load tests (Load Cases 3 through 7) were performed twice with Test Vehicle 2, crossing the bridge at a crawl speed. Data were

collected continuously during the entire time the truck was on the bridge. The seven load cases are shown in Figure 2.11.

Figure 2.10. Load Case 1 (stationary) during Test 1.

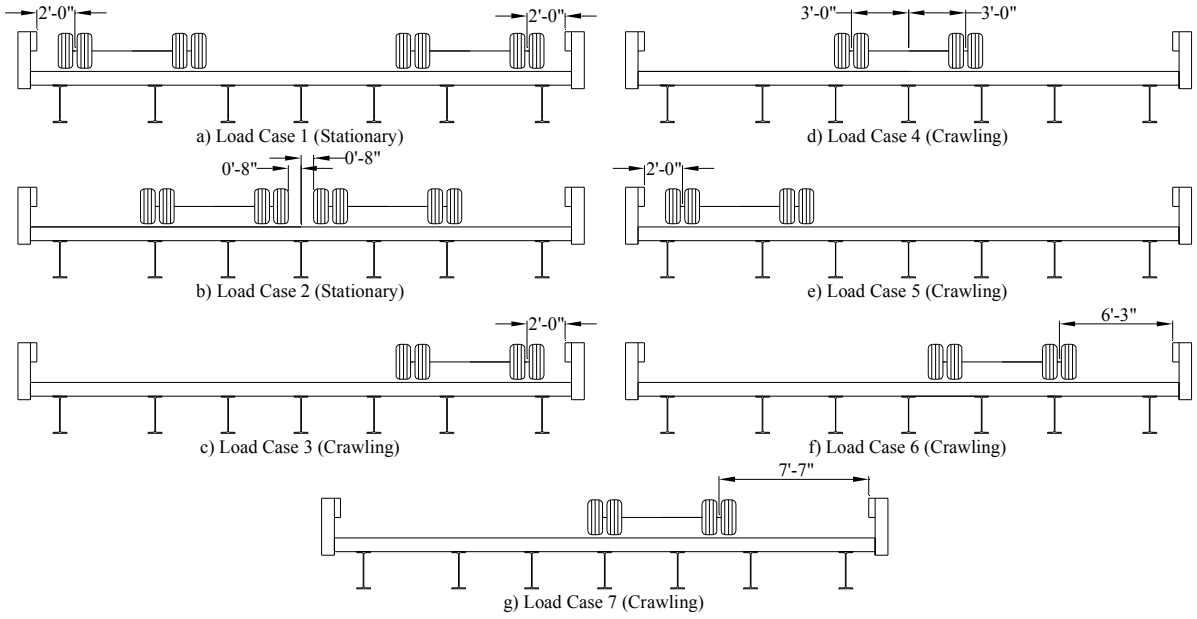

Figure 2.11. Load cases used in Test 1 and Test 2.

2.6. TEST RESULTS

In order to compare the test results to the design load of the bridge, a magnification factor must be implemented to approximate the effect of the test loads at the design load level. The field test results are multiplied by a factor equal to the ratio of the maximum moment induced by an HS20-44 design truck to the maximum moment induced by the test vehicles. The single lane loaded magnification factor for Test 1 is 1.267. This factor will be used for Load Cases 3 through 7. The magnification factor for the two lanes loaded conditions is 1.300 and was used in Load Cases 1 and 2. The single lane loaded magnification factor calculated for Test 2 used in Load Cases 3 through 7 is 1.263. The two lanes loaded magnification factor for Test 2 used for Load Cases 1 and 2 is 1.278.

2.6.1. Deflections

Figure 2.12 is a plot of maximum girder deflections for Load Cases 2 through 5 (labeled LC2, LC3, etc.) comparing both Test 1 and Test 2 on the same plot. The graph illustrates for these load cases (true for all load cases), the maximum deflections were greater in Test 2 than Test 1 despite a 0.15% decrease in the total truck weight. However, the shape of the curves for Test 2 and Test 1 are analogous to one another. The deflections for LC2 and LC4 are nearly symmetric about the center of the bridge due to the symmetry of the bridge and loading. In addition LC3 and LC5 are nearly mirrored images about the center of the bridge because of the loading in these two cases being opposite.

The maximum deflections during Test 1 for each girder ranged from 0.07 in. (L/7029) at Girder 1 to 0.085 in. (L/5788) at Girder 4. The AASHTO Specification [6] stipulates that the deflection due to service live load plus impact shall not exceed L/800 (0.62 in.) where

"L" is the span length of 41 ft. The deflections recorded during Test 1 were well below the specification limitation for all girders under all load cases. After applying the magnification factor of 1.267 for Girder 1 in Load Case 3 and the magnification factor of 1.300 for Girder 4 in Load Case 2, the maximum deflections of 0.09 in. and 0.11 in., respectively, are still well below the AASHTO limit.

The maximum deflections during Test 2 for each girder ranged from 0.075 in. (L/6560) at Girder 7 to 0.097 in. (L/5072) at Girder 4. After applying the magnification factors, the maximum girder deflection occurred in Girder 4 with a displacement of 0.124 in. (L/3968). The maximum deflections were much less than the AASHTO Specification [6] due to service live load plus impact. However, it should be noted that these tests were pseudo static in nature and it is possible that dynamic effects would result in larger deflections.

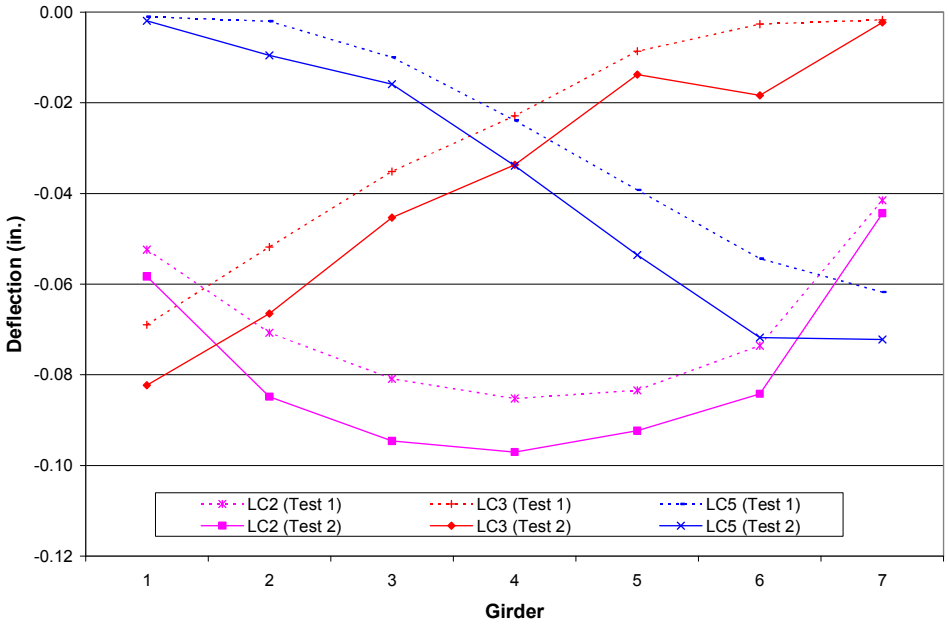

Figure 2.12. Maximum girder deflections at midspan from Test 1 and Test 2.

2.6.2. Girder Strains

Figure 2.13 displays the maximum bottom flange girder strains at midspan for both Test 1 and Test 2 for various load cases. As was the case for displacements, the strain values for Test 2 are greater than Test 1 with the exception of Girder 3. Also, the shape of the curves for Test 1 and Test 2 are similar to one another. It was assumed that the strain transducer for Girder 3 showed a malfunction in Test 1. The following graph illustrates that the assumption was most likely correct. It is also noted in Figure 2.13, Load Cases 3 and 5 have almost the same value for the center girder because of the symmetry in both the loading and the bridge. Also, the strain plots are very similar to the displacement curves (Figure 2.12) except mirrored about the x-axis.

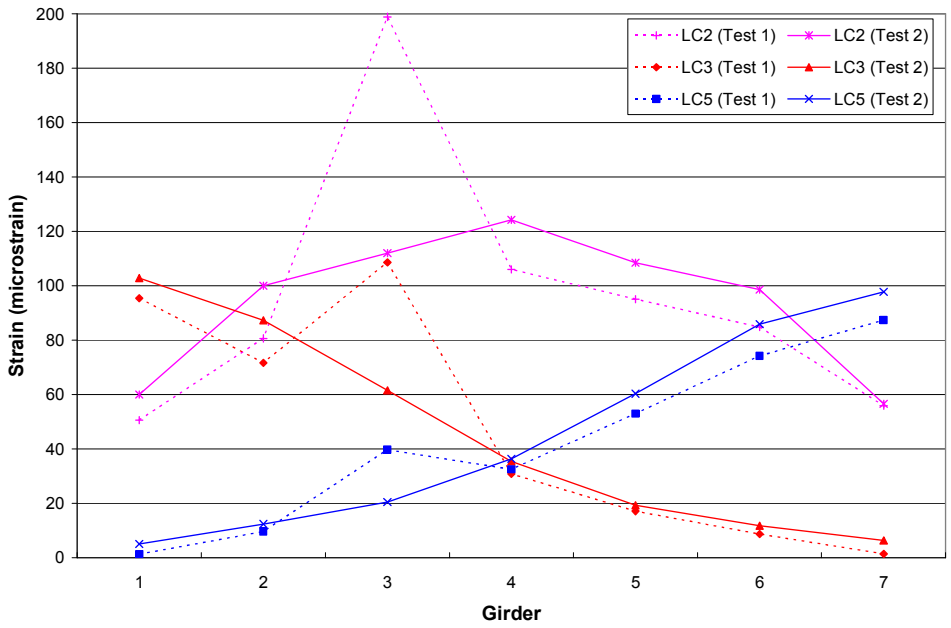

Figure 2.13. Maximum girder strains at midspan from Test 1 and Test 2.

The maximum midspan flexural strain (107 microstrain) during Test 1 (disregarding Girder 3 due to the malfunction) occurred in the bottom flange of Girder 1 under Load Case

1. The correlating maximum tensile stress in the girder bottom flange (assuming E_s=29,000 ksi) was 3.1 ksi, which is approximately 10 percent of the yield stress of the girders (30 ksi). After applying the magnification factor of 1.3, the maximum two lanes loaded stress is 4.03 ksi. The maximum strain of 95 microstrain for Test 1 under a single lane loaded occurred during Load Case 3 at Girder 1. Applying the single lane loaded magnification factor of 1.267, the maximum strain is 121 microstrain and a correlating tensile stress of 3.5 ksi.

The maximum strain values in Test 2 for the bottom flange girders at midspan ranged from just under 100 microstrain in Girder 6 to the highest strain of 124 microstrain in the center girder (Girder 4) in Load Case 2. The maximum tensile stress associated with the maximum strain in Girder 4 (assuming E_s=29,000 ksi) was 3.6 ksi, which is 12% of the yield stress of 30 ksi. After applying the magnification factor, the maximum strain is 158 microstrain (maximum stress of 4.6 ksi) in Girder 4.

2.6.3. Concrete Deck Principal Strains and Stresses

The original strains were measured using three strain transducers oriented in a 0-45-90 degree rectangular rosette. From these three measured strains, the principal strains were calculated using Equation 2.3:

$$\varepsilon_1, \varepsilon_2 = \frac{\varepsilon_x + \varepsilon_y}{2} \pm \sqrt{\left[\left(\frac{\varepsilon_x - \varepsilon_y}{2}\right)^2 + {\varepsilon_{xy}}^2\right]} \tag{2.3}$$

Where:

$\varepsilon_1, \varepsilon_2$ = principal strains

ε_x = strain in the longitudinal direction (0-degrees)

ε_y = strain in the transverse direction (90-degrees)

$$\varepsilon_{xy} = \varepsilon_{45} - \frac{\varepsilon_x + \varepsilon_y}{2} \text{ (shear strain)}$$

From these principal strains, the principal stresses are then calculated using Equations 2.4:

$$\sigma_1 = \frac{E}{1-\nu^2}(\varepsilon_1 + \nu\varepsilon_2) \qquad \sigma_2 = \frac{E}{1-\nu^2}(\varepsilon_2 + \nu\varepsilon_1) \qquad \tau_{\max} = \frac{\sigma_1 - \sigma_2}{2} \text{ or } \frac{\sigma_1}{2} \tag{2.4}$$

Where:

E = Young's Modulus (Assumed 3372 ksi)

ν = Poisson's Ratio (Assumed 0.20)

As previously noted, the design compressive strength of the concrete was 3,500 psi with the actual compressive strength at 56 days over 6,100 psi. The maximum tensile principal stress calculated from the strain transducer rosettes in Test 1 was 106 psi at point A in Figure 2.6. This maximum value occurred during Load Case 2 (two trucks near centerline at midspan). At the same location (point B in Figure 2.7) and load case, the maximum tensile principal stress during Test 2 was 185 psi. Both calculated stresses were below the assumed modulus of rupture for the concrete, (237 psi) [5] and the actual tested flexural strength of the FRC (624 psi).

The maximum tensile principal stress computed for a single truck load case in Test 1 was 95 psi, or 120 psi after applying a magnification factor of 1.267. The location of this stress was at point A in Figure 2.6 and occurred during Load Case 7. The maximum tensile principal stress computed for a single truck load case during Test 2 occurred in Load Case 4 and at point C in Figure 2.7. The computed value was 157 psi, and the magnified value after multiplying by 1.263 was 198 psi. This maximum tensile principal stress for Test 1 was

much lower than Test 2 because the location of the stress in Test 2 was at a location that was not instrumented for Test 1. All the maximum tensile principal stresses after applying the magnification factor were still below the assumed modulus of rupture for the concrete (237 psi) [5] and the tested flexural strength of the FRC (624 psi).

The tensile principal stresses from Test 1 and Test 2 differ by a considerable amount. The 185 psi tension value from Test 2 occurred at a sharp spike in the plot which is associated with the truck movement. The largest sustained tensile principal stress from Test 2 is still considerably higher than Test 1 with a value of 170 psi. However, these disparities my have occurred due to the exact location and accuracy of placing the transducers at the specific 0-45-90 degree angles. In addition, extensions were not used on the strain transducers so the measurements may be affected by local imperfections and hairline cracks.

2.6.4. Transverse Steel Strap Strains and Stresses

The maximum tensile strain in a transverse steel strap during Test 1 occurred between Girders 4 and 5 at midspan with a strain of 71 microstrain, resulting from Load Case 2. The corresponding maximum tensile stress in the straps (assuming Es=29,000 ksi) was 2.1 ksi or 2.73 ksi after magnification, which is less than eight percent of the yield stress of the straps (36 ksi). The maximum tensile strain in a transverse steel strap during Test 2 was 49 microstrain, resulting from Load Case 7 in the strap between Girders 2 and 3 at midspan. The corresponding stress in the straps (assuming Es=29,000 ksi) was 1.4 ksi, which is less than four percent of the yield stress of the straps (36 ksi). Incorporating the magnification factor of 1.263, the maximum strain was 61 microstrain and the maximum stress was 1.8 ksi.

2.6.5. Comparing Transverse Steel Strap Strain with Concrete Deck Strain

A typical relationship between the transverse concrete strain and tensile transverse steel strap strain at midspan is shown in Figure 2.14 for Load Case 6 in which the wheel of the truck passes directly over these transducers. The strain transducers were located at the bridge midspan between Girders 3 and 4. The strains measured at these locations correlate with one another as expected. The first local maximum indicates the strain when the front axle passes over the transducers and the other two maximums are associated with the rear axles. As the concrete deck becomes strained in tension, the transverse steel strap carries a similar amount of strain, much like reinforcing bars in conventional deck systems.

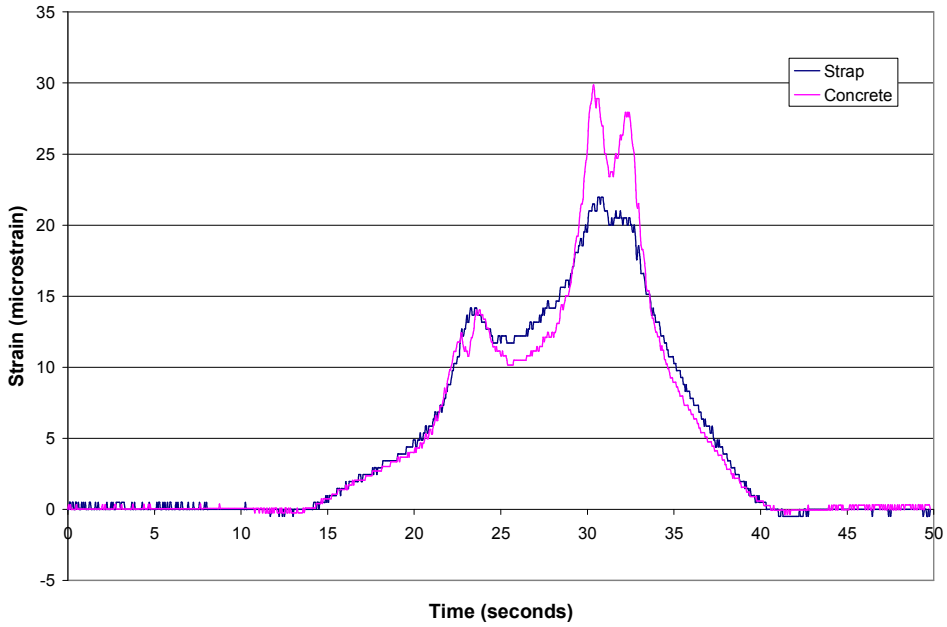

Figure 2.14. Transverse steel strap strain and concrete deck strain (Load Case 6) located between Girders 3 and 4 at midspan from Test 2.

2.6.6. Distribution Factors

Experimental load fractions were calculated from the measured girder deflections in the structure at midspan using Equation 2.5.

$$LF_i = \frac{\Delta_i}{\sum_{i=1}^{n} \Delta_i} \tag{2.5}$$

Where: LFi = load fraction of the ith girder (lanes/girder).

Δi = deflection of the ith girder.

$\sum \Delta i$ = sum of girder deflections.

n = number of girders.

Experimental distribution factors were then calculated from the load fractions by superimposing the load fractions from two single lane loaded cases (Load Cases 3 through 7) or doubling the values for the two lanes loaded cases (Load Cases 1 and 2). The load distribution factors were compared to AASHTO design distribution factors [6]. The maximum distribution factors and the bridge design code distribution factors are shown in Figure 2.15. Bridge design code distribution factors for two lanes loaded are labeled as "Design" and the corresponding load cases are labeled such the LC1 is calculated by doubling Load Case 1 and LC3 + LC5 is the effective result of superimposing Load Case 3 and Load Case 5.

The experimental distribution factors are all less than the AASHTO factors with the exception of LC2 which was within one percent difference of the AASHTO value; however, the AASHTO [6] factors assume equal girder spacing. The unequal spacing of the exterior girders could account for some of the differences between the design values and the measured values. Another possible cause for the differences is the relatively low deflections that were

measured on the bridge. Because the loads for Load Cases 3 through 7 were moving, there may have been some influence of vibration or impact of the load on the distribution of the loads. A small change in girder deflection due to vibration or impact could be significant enough to change the distribution factors computed from the data. Due to the low girder stresses calculated from the load test data, the girders are adequate despite the slightly un-conservative estimates of load distribution.

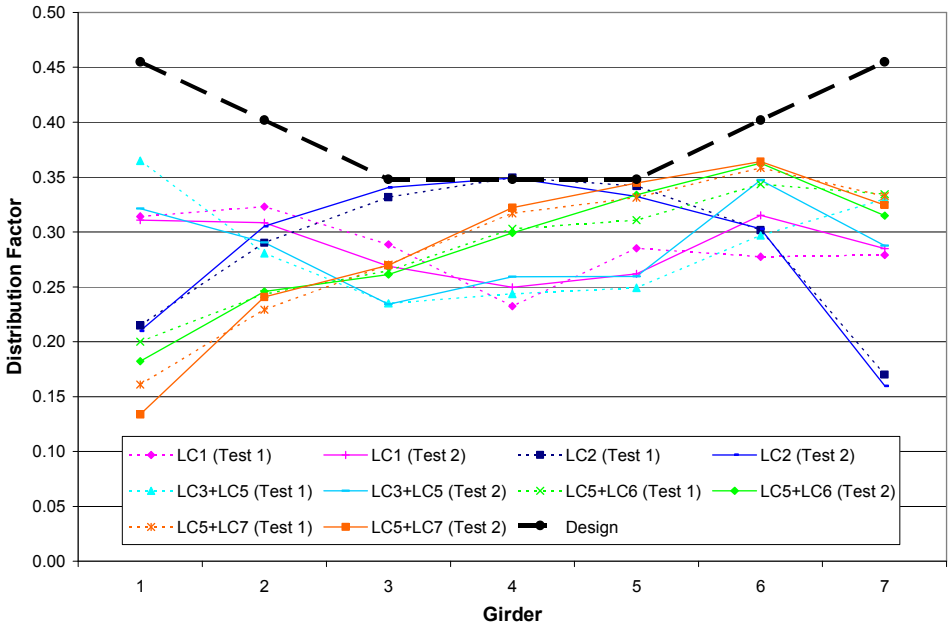

Figure 2.15. Experimental and AASHTO Distribution Factors from Test 1 and Test 2.

2.7. CONCLUSIONS

This paper presented the design, construction, and test results for the first SFD bridge built in the United States. Based on the results of the two live load field tests, the following conclusions can be made:

1. Girder deflections at midspan were well below the AASHTO L/800 limitation for

serviceability.

2. All of the computed stresses in the girders and transverse steel straps were 15% or less than the yield stress of the steel.
3. No cracks were observed in the concrete deck at the time of testing and all computed principal stresses in the concrete deck were below the cracking stress of the concrete. Previous SFD demonstrations have shown longitudinal cracking; however, installing the GFRP grid in the TCB appears to have been a key component in preventing longitudinal cracking.
4. The results from both tests displayed a correlation between the concrete deck and the transverse steel straps verifying the effectiveness of the straps.
5. The experimental load distribution factors were in good agreement with the AASHTO distribution factors used for design. All experimental load distribution factors were less than the AASHTO factors except for Load Case 2 which was within one percent difference.
6. Overall, the single-span, steel girder bridge with a composite SFD system performed well during the live load field tests.

There is no indication of any reduction in structural performance due to the design of the bridge deck. Therefore, the SFD system should be recommended as an alternative design to the conventional steel reinforced deck; however, to adequately monitor the durability of the SFD, continued testing should be performed. These investigations and demonstrations are crucial to the acceptance and future implementation of a SFD system. Also, future monitoring and cost analysis of the SFD would confirm the expected increase in durability and lifespan while generating savings in maintenance expenses. Any additional tests would

also expand the SFD system data base. In order to fully realize the benefits of utilizing the SFD system, the bridge deck should be truly steel-free. Future applications should investigate ways to replace the steel in the overhang portion of the deck with alternative reinforcement materials that are corrosion resistant, such as FRP bars. Finally, the CHBDC may require an overly conservative requirement for the transverse steel straps by disregarding the stiffness of the entire system. Future testing should investigate the recommended strap area used for transverse restraint in order to maintain adequate lateral stiffness and produces the desired internal arching action.

2.8. REFERENCES

1. Thornburn, J., and A. Mufti. Design Recommendations for Externally Restrained Highway Bridge Decks. *Journal of Bridge Engineering,* July/August 2001, pp. 243-249.
2. Ventura, C., and S. Cook. Testing of a Steel-Free Concrete Bridge. *Experimental Techniques*, November/December 1998, pp. 39-42.
3. OHBDC (Ontario Highway Bridge Design Code). Ministry of Transportation of Ontario, Downsview Ontario, 1991.
4. Mufti, A., L. Jaeger, B. Bakht, and L. Wegner. Experimental Investigation of Fibre-Reinforced Concrete Deck Slabs Without Internal Steel Reinforcement. *Canadian Journal of Civil Engineering*, Vol. 20, 1993, pp. 398-406.
5. Canadian Highway Bridge Design Code, *1st edition*, Toronto, Ontario, Canada. December 2000.

6. AASHTO (American Association of State Highway and Transportation Officials), *Standard Specifications for Highway Bridges, 16th edition*, Washington, D.C., 1996.
7. Iowa Department of Transportation, Standard Specifications for Highway and Bridge Construction, Ames, IA, 1997.
8. AISC (American Institute of Steel Construction, Inc.), *Manual of Steel Construction, Load and Resistance Factor Design, 2nd edition*, Chicago IL, 1998.

CHAPTER 3. PERFORMANCE EVALUATION OF A SINGLE-SPAN ULTRA-HIGH PERFORMANCE CONCRETE GIRDER BRIDGE

A paper to be submitted to the *Journal of Bridge Engineering*

Mark T. Giesmann, Brian E. Degen,

Brent M. Phares, Terry J. Wipf, "Sri" S. Sritharan

3.1. ABSTRACT

Researchers at the Bridge Engineering Center at Iowa State University have researched, designed, and tested the first known bridge in the United States that has implemented a recently developed material called Ultra-High Performance Concrete (UHPC). UHPC has been shown to have superior material characteristics with compressive strengths up to 30,000 psi and tensile strengths up to 1,700 psi, lending itself to be a desirable construction material. In the fall of 2005, the 110 ft single-span prestressed UHPC girder bridge was constructed in Wapello County, Iowa. This paper describes the design and construction of the UHPC bridge and then presents the results of two live load field tests conducted on the completed bridge to evaluate the structural performance.

3.2. INTRODUCTION

In 2003, the Iowa Department of Transportation (Iowa DOT) and Wapello County, Iowa began planning for a bridge replacement project. The need and timing for a bridge replacement presented an opportunity to use a newly developed material called Ultra-High Performance Concrete (UHPC). Partially funded through the Federal Highway Administration's (FHWA) Innovative Bridge Research and Construction (IBRC) program,

this bridge became the first UHPC bridge constructed in the United States.

The research conducted in this project initially included designing, documenting, and constructing the first UHPC bridge in the United States. Concurrently, research was conducted to perform a performance evaluation to ensure the viability of the UHPC bridge design. Two other aspects were investigated further to aid in design: defining of material properties and understanding of flexural behavior. In order to obtain information in these areas, several tests were carried out including material testing, large-scale laboratory flexure testing, large-scale laboratory shear testing, large-scale laboratory flexure-shear testing, small-scale laboratory shear testing, and field testing. Background, design, construction, and large-scale laboratory flexure testing of the UHPC bridge is presented here; however, the focus of this paper is to present the results of two live load field tests. Refer to Wipf et al [1] for information on the complete UHPC project.

In addition to conventional concrete, UHPC typically consists of silica fume, fly ash, retarder, and superplasticizer to increase the material's strength and workability. Also, small fibers (steel or organic) are randomly mixed in to increase both the material's tensile strength and its ductility. However, UHPC does not include coarse aggregate filler material, which is generally a weak component. The compressive strength of UHPC generally ranges from 16,000 psi up to 30,000 psi and the tensile strength, usually neglected in concrete, can be as high as 1,700 psi. A typical mix design of UHPC is described in Table 3.1. The UHPC used in this project is a specific brand manufactured by Lafarge North America and is know as Ductal®.

The attributes of UHPC make it a beneficial construction material. Due to the increase in compressive and tensile strengths, UHPC structural components are lighter and

smaller in size. The high density of the UHPC also makes the material impermeable to water and chlorides, thus protecting steel reinforcement from corroding and making UHPC highly durable.

Table 3.1. Typical UHPC material composition [2].

Material	Amount (lb/cubic yard)
Portland Cement	1200
Fine Sand	1720
Silica Fume	390
Ground Quartz	355
Superplasticizer	51.8
Accelerator	50.5
Steel Fibers	263
Water	184

3.3. DESIGN AND CONSTRUCTION

The first UHPC bridge in the United States was constructed in Wapello County, Iowa during the fall of 2005. Design of the bridge was completed cooperatively between the Iowa DOT, Wapello County, and ISU. The bridge has no horizontal curve, vertical curve, nor skew. The cross section of the bridge as a whole is shown in Figure 3.1. The deck has a 2% transverse crown from the peak at the centerline of the roadway. The deck reinforcement consists of transverse and longitudinal steel in both the top and bottom of the deck. The transverse steel has top cover of 2.5 in. and bottom cover of 1 in. with the longitudinal steel placed inside of the transverse steel. The #7 transverse bars are spaced at 9 in. across the width of the deck in both the top and bottom of the slab. In addition, #5 transverse bars spaced at 9 in. between the #7's are in the top of the deck in the outer 6.67 ft of the deck to further strengthen the overhang. The longitudinal steel consists of #5 bars spaced at 1 ft between the beams with the top and bottom reinforcement staggered in spacing. Similar reinforcement exists in the overhang of the deck. There is one diaphragm located at midspan

of the bridge consisting of two C15x33.9 steel sections with one connecting each of the outer beams to the center beam at the mid-depth of the beams. Conventional Iowa DOT integral abutments with wingwalls and open guard rails were used for this bridge.

The three bridge beams used on this project were modified slightly from the Iowa DOT Bulb Tee C standard with the dimensions shown in Figure 3.2. The beams are 111 ft long with a 110 ft span. Note the solid five strands that are aligned vertically near the top of Figure 3.2.a. These are the prestressed harped strands that decline linearly from the end cross section (Figure 3.2.a.) to the midspan cross section (Figure 3.2.b.) over a distance of 44.5 ft as shown in Figure 3.3. Within the central 22 ft of the beam, all the strands run horizontally and are located as shown in the midspan cross section. There are #5 reinforcing bars with two legs in the top of the bridge beams in order to connect the deck and beams for composite action and resist horizontal shear. The spacing of the horizontal shear bars are shown in Figure 3.3. The last 3.5 ft of the beams on both ends have eight strands that are debonded in the bottom flange. The last 6.5 ft of the beams on both ends have 16 strands that are debonded in the bottom flange. Debonding was used in order to reduce the stresses at the flange-web interface. No shear reinforcement is present within the beams because it has been replaced by steel fibers. The nearly completed bridge is shown in an elevation view in Figure 3.4. Refer to Degen [3] for complete design calculations and construction documentation of the UHPC bridge.

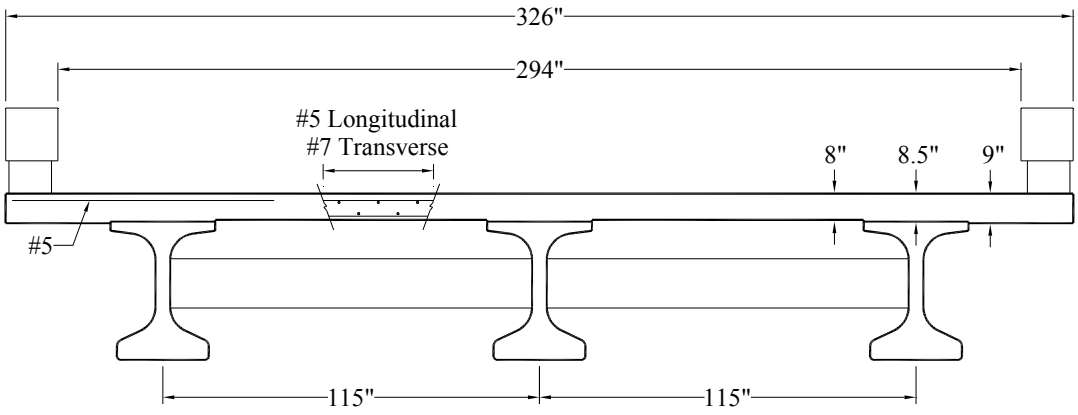

Figure 3.1. Cross section of Wapello County UHPC bridge.

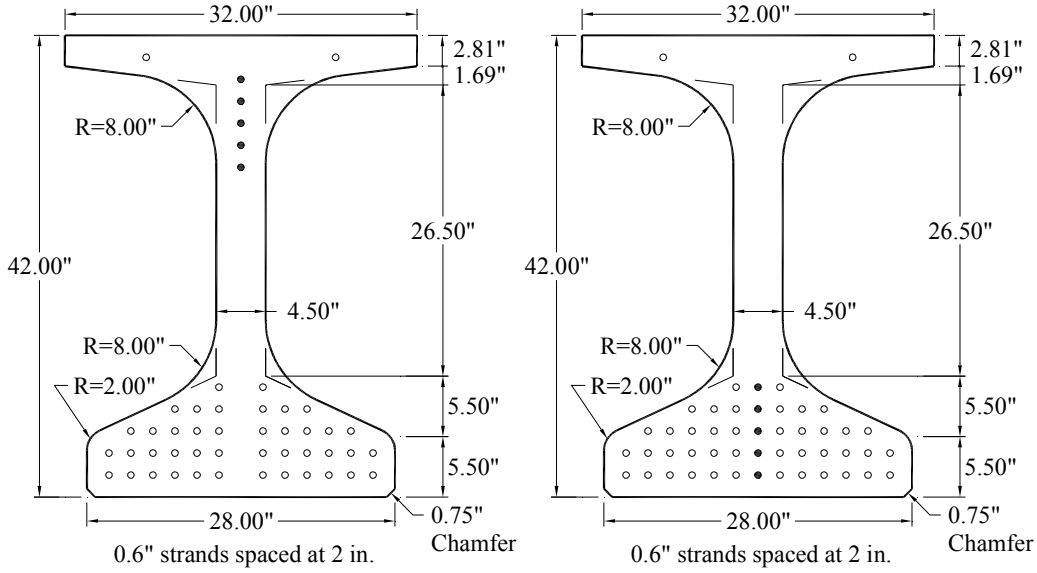

a. End cross section. b. Midspan cross section.

Figure 3.2. Cross sections of Wapello County UHPC bridge beams.

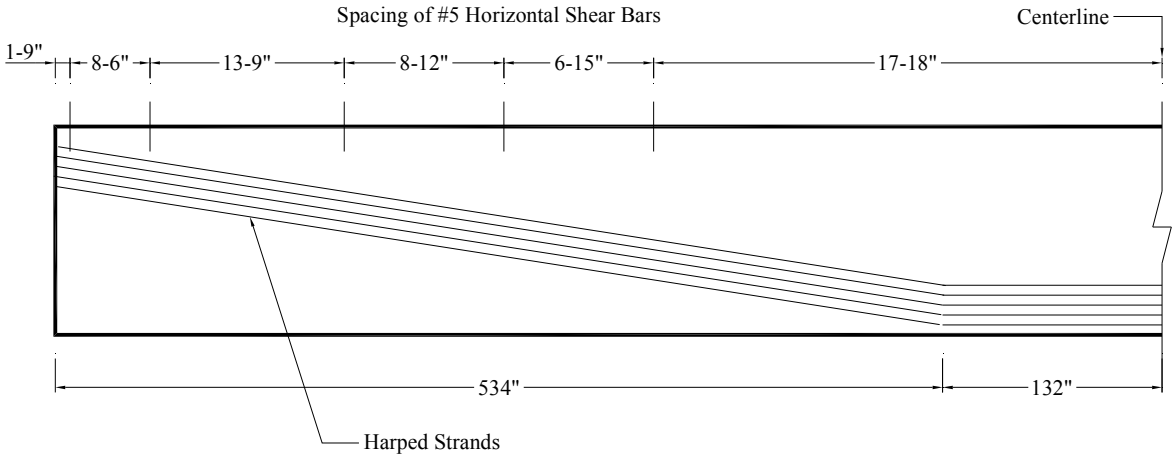

Figure 3.3. Elevation of Wapello County UHPC bridge beams.

Figure 3.4. Elevation of Wapello County UHPC bridge.

3.4. LARGE-SCALE LABORATORY FLEXURE TESTING

Large-scale laboratory testing was completed by Brian Degen at ISU to collect information about the structural performance of UHPC. The flexure test provided information about the service limit state capacity of the beam and prestress losses.

3.4.1. Test Specimen

The cross sections of the large-scale laboratory test beam were the same as for the bridge beams shown in Figure 3.2. The total length of the test beam was 71 ft with the harped stands varying linearly between the two cross sections which are 28.5 ft apart. The central 14 ft of the beam had the midspan cross section shown in Figure 3.2.b. Debonding was used in the same manner as previously described for the bridge beams. The test beam design was configured with the same cross section as the Wapello County, Iowa bridge beams and limited to a practical length and weight for the ISU Structural Engineering Laboratory.

3.4.2. Flexural Testing Configuration

The flexure test setup used in this work consisted of a 70 ft span with four applied point loads centered over the midspan, creating a constant moment region of approximately 64 in. Figure 3.5 shows the test setup.

To quantify the response of the test beam, several different types of instrumentation were used. During testing, a Megadac System and a Fiber Optic Interragator running at 1 Hz were used to collect data. During the flexure test, top flange and bottom flange strains were measured at the midspan using linear strain gages and midspan deflections were measured

using string potentiometers. In addititon, four load cells were used to measure loads (L1, L2, L3, L4) and three DCDT's were used to measure strand slip.

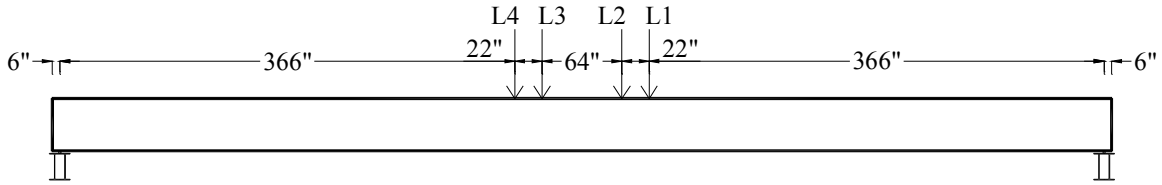

Figure 3.5. Large-scale flexure test setup diagram.

3.4.3. Test Procedure

Flexural testing was performed on May 11th, 2005. Two sequences of loading were applied. During the first sequence of loading a total load of 237.4 kips was applied to the beam at which point the beam was inspected for flexural cracks at midspan and revealed one very small hairline crack near the beam midspan which was subsequently verified to be a crack during the second sequence of loading. Additional loading was applied to an approximate total load of 243 kips and 3 in. of midspan deflection. At this point, the beam was unloaded.

A second sequence of loading was then applied to the beam. The beam was first loaded to a total load of 256 kips and the beam was inspected for flexural cracks and 13 hairline cracks spaced at about 6 in. were discovered on the bottom flange of the beam within the constant moment region. Loading was resumed to a total load of 265 kips and 3.2 in. of deflection when the final inspection of the beam took place where one new crack was found nearly at the midspan of the beam. All 14 cracks ran transversely across the entire bottom flange of the beam. The cracks were marked with typical examples shown in a close up view on the bottom flange of the north face of the beam in Figure 3.6. Testing was halted at this

point to maintain the structural integrity of the beam for shear testing. It should be pointed out that the maximum applied moment is slightly under the service load condition and well under the ultimate load condition for the composite bridge beam and deck system.

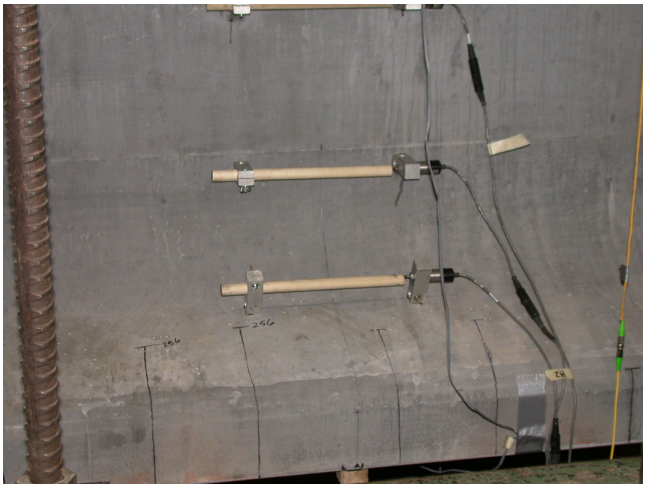

Figure 3.6. Flexural cracks on bottom flange at midspan during large-scale flexure test.

3.5. LARGE-SCALE LABORATORY FLEXURE TEST RESULTS

The primary purpose of the flexure test was to provide reassurance to the design engineer that the beam had sufficient capacity for implementation in the first United States UHPC bridge in Wapello County, Iowa. This was achieved by reaching a load level above the expected service loads before cracking occurred. The service level is determined by a simple summation of external moments required to be resisted by the bridge beam which included moment from the bridge deck, future overlay, barriers, and the live load as required by code. Using the effective width of the bridge deck according to AASHTO [4], the bridge beams have a larger section than the test beam and therefore can resist even more moment. As can be seen in Figure 3.7, where Gage #11 and Gage #12 are top flange and bottom flange

strains respectively, the total load when non-linearity occurs at cracking was 237.4 kips which corresponds to a moment of 3,730 ft-k, not including the beam self-weight. Using this information and the additional effective width of the slab, a service moment capacity of the bridge beam can be determined which should be larger than the applied service moment as shown in Table 3.2. The same type of process was carried out for the ultimate limit state. However, test data for this beam did not reach this level, and therefore, the quantities shown in Table 3.2 are based off of analysis rather than testing.

In addition, the flexure test was useful for estimating the amount of prestressing in the test beam. By using the applied moment at which cracking occurred, the prestressing force was estimated to be 1517 kips (27.2% loss) experimentally using a simple linear stress analysis. The amount of prestressing determined experimentally was also compared with traditional calculations made during initial design. The losses that were accounted for are the initial relaxation, elastic shortening, shrinkage, creep, and secondary relaxation. These loss calculations are described by AASHTO [4] and are documented in Degen [3]. The calculated analytical prestressing force after losses is 1450 kips (30.4% loss) which correlates fairly well with the experimental results.

Several instruments recorded data during the test to ensure that the beam was behaving as expected. The deflection at several locations could be accurately calculated within the linear range when using the unit load method. Figure 3.8 shows the midspan experimental and analytical deflection. As well, the stresses within the beam could be predicted accurately. For instance, in Figure 3.9 the stresses at midspan under a total load of 237 kips are shown to be accurate and uphold the assumption that plane sections remain

plane. In addition, three strands were monitored for slip. One gage indicated a rapid increase in slip to 0.005 in. at the maximum load as shown in Figure 3.10.

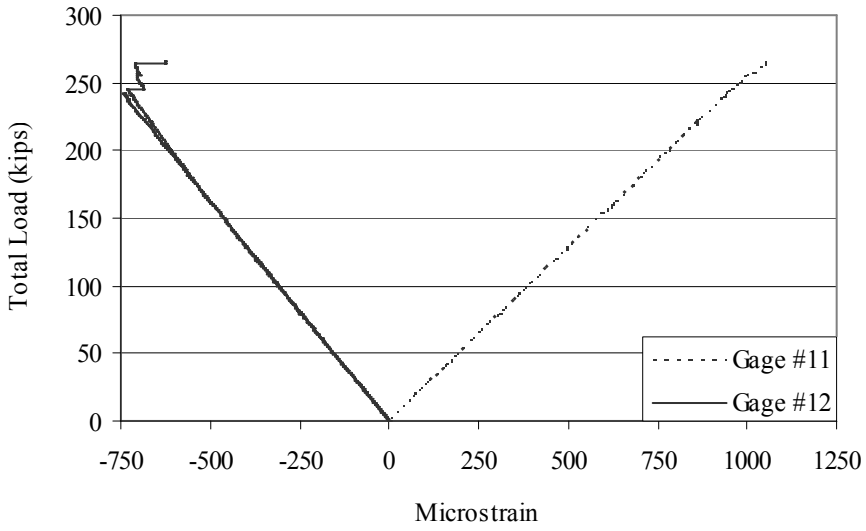

Figure 3.7. Strain at midspan during large-scale flexure test.

Table 3.2. Comparison of large-scale flexure test capacities to applied bridge moments.

Limit State	Experimental Moment Capacity of Test Beam (ft-kips)	Analytical Moment Capacity of Bridge Beam (ft-kips)	Applied Moment on Bridge Beam (ft-kips)
Service Level	3,730	4,760	4,624
Ultimate Level	N/A	7,620	7,350

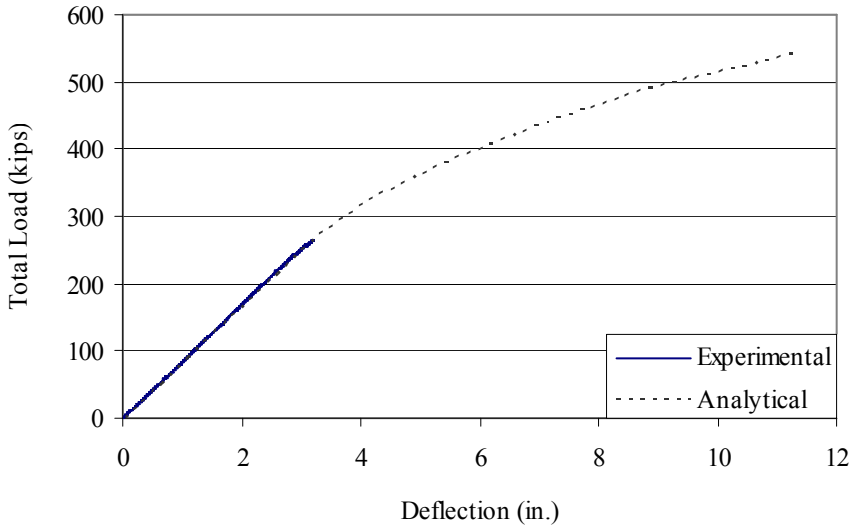

Figure 3.8. Deflection at midspan during large-scale flexure test.

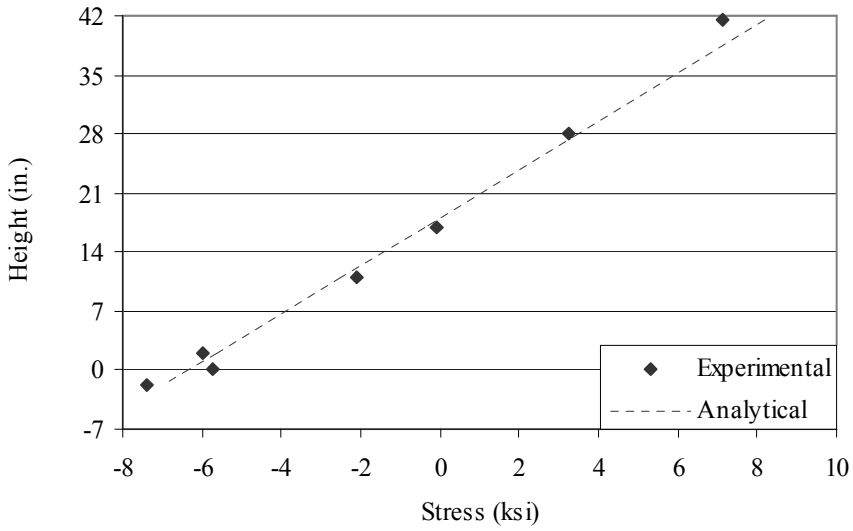

Figure 3.9. Longitudinal live load stresses at cracking of large-scale flexure test beam.

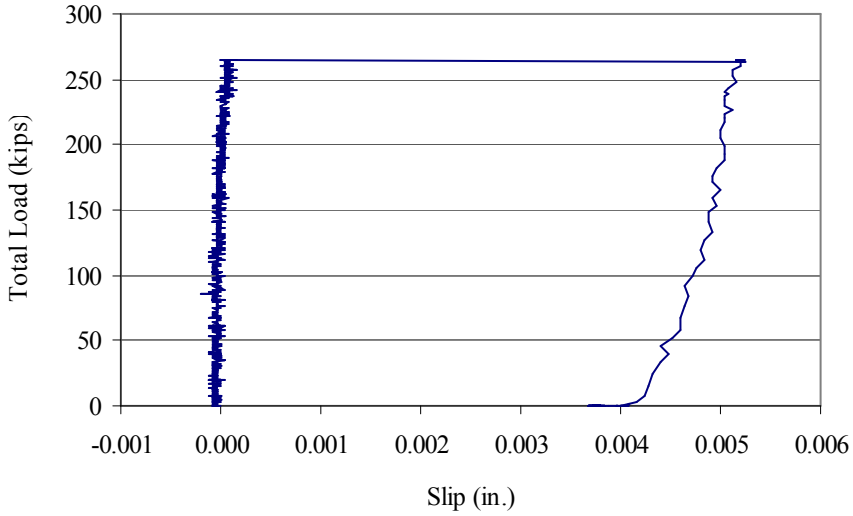

Figure 3.10. Strand slip during large-scale flexure test.

3.6. LIVE LOAD TESTING

The purpose of the live load testing was to determine the structural performance of the UHPC bridge and to make comparisons to design assumptions. Two tests were

conducted, one on August 23rd, 2006 (Test 1) and the other on June 7th, 2007 (Test 2) using essentially the same test configuration.

3.6.1. Test Configuration

In order to get an overall structural performance profile, Bridge Diagnostics, Inc. (BDI) Intelliducers and Structural Testing System (STS) were used to measure longitudinal live load strains. Figure 3.11 shows two typical BDI strain transducers attached to the top flange and concrete deck of the structure at one particular location.

Figure 3.11. BDI strain transducers attached to concrete.

At the midspan, south quarter span, and 42 in. from the south abutment, BDI strain transducers were attached in the longitudinal direction to the underside of the bottom flanges and near the top edge of the top flanges of each beam. Strain transducers were also attached to the underside of the bridge deck near the top flange in the longitudinal direction. A total of 18 BDI strain transducers were attached to the three girders and another nine were attached to the concrete deck. Figure 3.12 shows the instrumentation plan used for both live load tests.

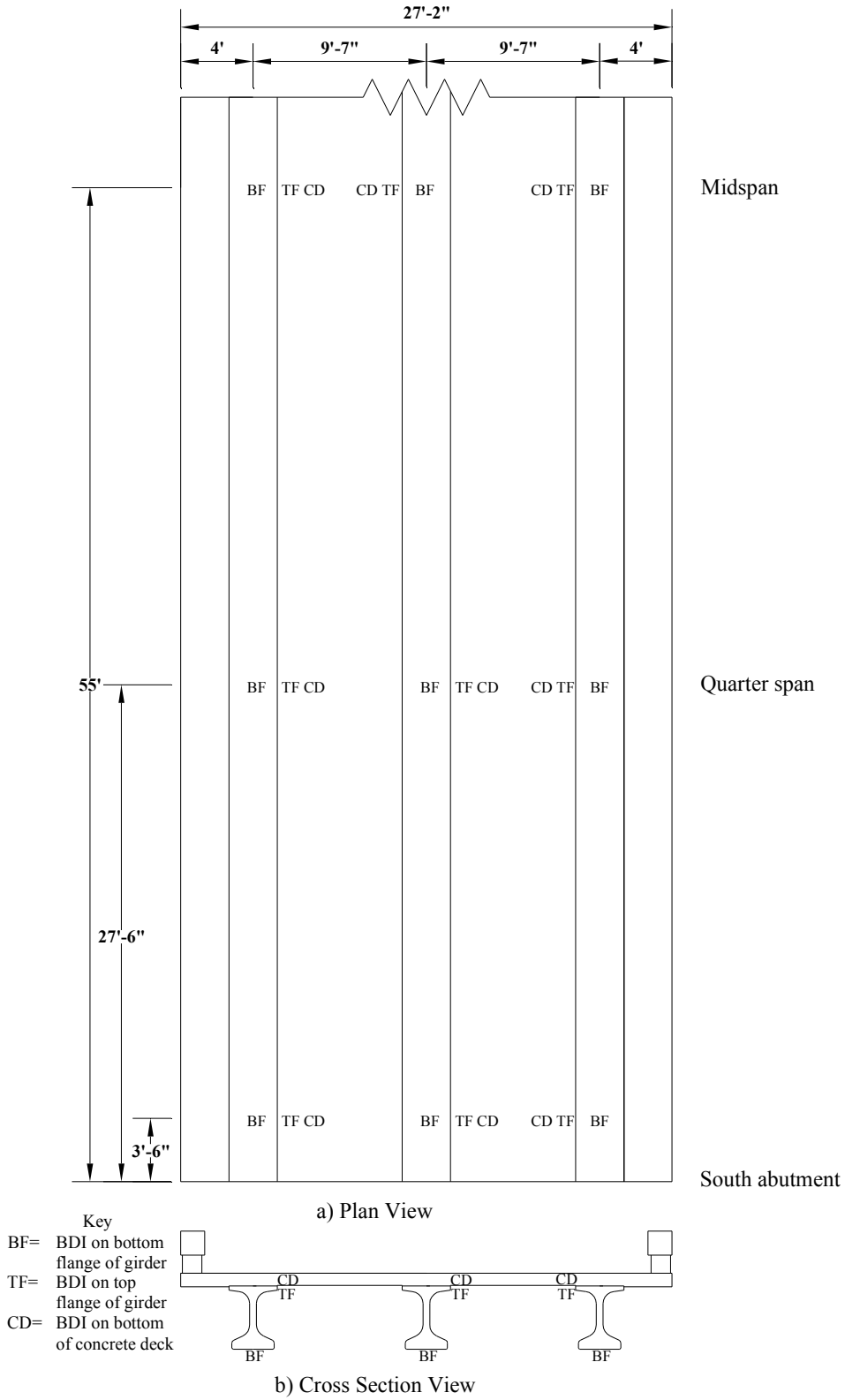

Figure 3.12. Location of BDI strain transducers used during both tests.

3.6.2. Test Procedure

The bridge was loaded using a loaded tandem-axle dump truck provided by Wapello County. The total weight of the loaded tandem-axle dump truck for Test 1 and Test 2 was 54,060 lbs and 51,840 lbs, respectively, as shown in Tables 3.3. Figure 3.13 shows the configurations of the test vehicles used for each test.

The bridge was loaded under five pseudo-static load cases and four dynamic load cases. The pseudo-static load cases (Load Case 1 through Load Case 5) were preformed with the test vehicle crossing the bridge at a crawl speed. The dynamic load cases (Load Case 6 through Load Case 9) were performed at speeds varying between 20 and 35 mph. Data were collected continuously during the entire time the truck was on the bridge. The load cases are shown in Figure 3.14.

3.6.2.1. Pseudo-Static Loading

The pseudo-static load cases were each run twice using the test vehicle. Load Case 1 and Load Case 5 placed the wheel line of the truck 2 ft from the guard rail. The 2 ft offset was selected because current AASHTO [4] specifications dictate this as the minimum offset of the vehicle wheel line from the edge. Load Case 2 and Load Case 4 were selected to place the wheel line directly over the center girder. The truck was centered on the bridge for Load Case 3.

3.6.2.1. Dynamic Loading

The dynamic load cases were also each run twice. Load Case 6 and Load Case 7 were placed at the same location as Load Case 1 (2 ft from guard rail) with the target truck speeds of Load Case 6 being 20 mph and Load Case 7 being 35 mph. Load Case 8 and Load Case 9 were placed at the same location as Load Case 3 (truck centered) with the target truck speeds

of Load Case 8 being 20 mph and Load Case 9 being 35 mph. Note that the 35 mph truck speed was difficult to reach since the roadway surface was gravel and there was a curve in the road just prior to the bridge.

Table 3.3. Summary of test vehicle's configurations and weights.

	Dimensions			Front Axle Weight	Rear Axles Weight	Total Weight
	'a'	'b'	'c'	(lbs)	(lbs)	(lbs)
Test 1	7'-2"	17'-3"	4'-7"	17,280	36,780	54,060
Test 2	7'-1"	15'-10"	4'-5"	15,820	36,020	51,840

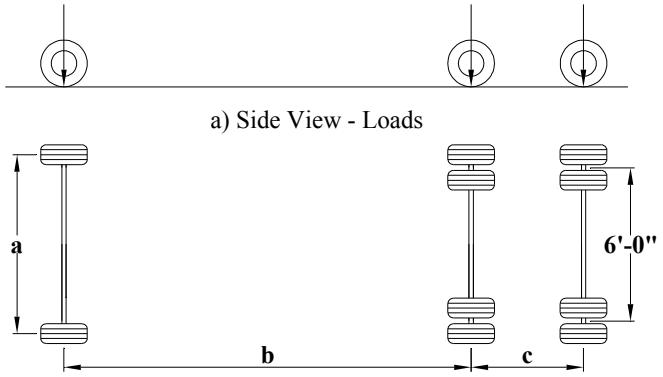

c) Tandem truck used during Test 2

Figure 3.13. Test vehicle configuration.

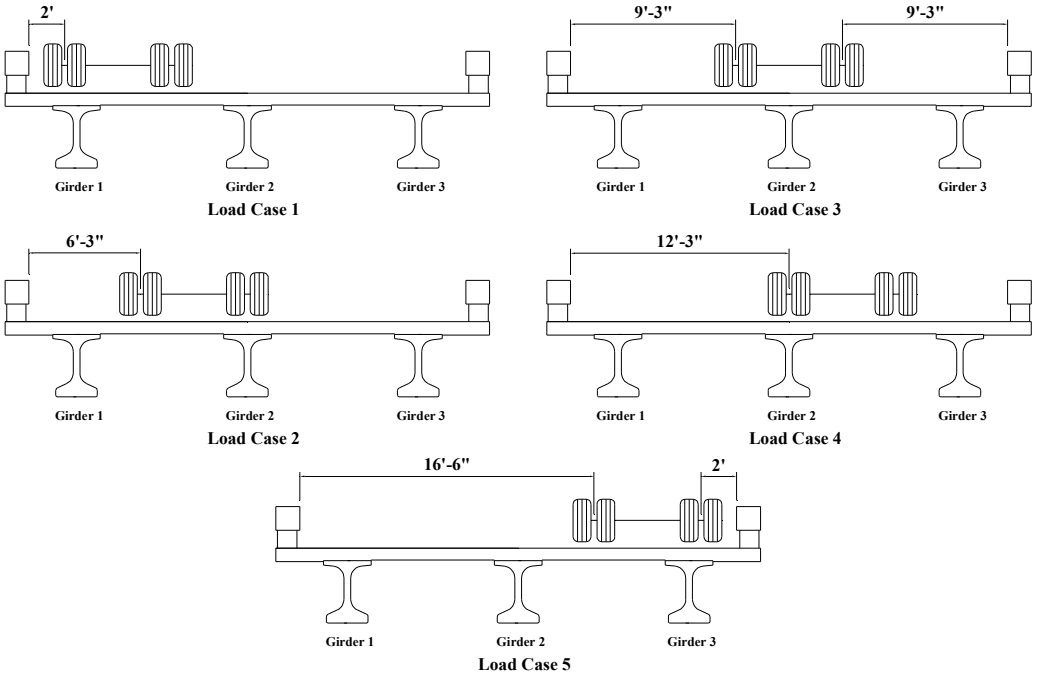

Figure 3.14. Truck positions used in the live load tests.

3.7. LIVE LOAD TEST RESULTS

In order to compare the experimental results to the design condition, a magnification factor must be implemented to approximate the effect of a design vehicle. The ratio of the weight of the design vehicle, HS20-44, to the test vehicle was used as an approximate magnification factor. Note that this magnification factor was applied to all strain values presented here. The magnification factors used for Test 1 and Test 2 were 1.33 and 1.39, respectively.

3.7.1. Bottom Flange Midspan Girder Strains

Figure 3.15 shows the maximum tensile strain in the girder bottom flange at midspan for the static Load Cases 1 through 5 during Test 1. The maximum midspan flexural strain

during Test 1 (70.8 microstrain tension) occurred in the bottom flange of girder 1 for Load Case 1. The corresponding maximum tensile stress in the girder bottom flange (assuming E_c=7820 ksi) was 554 psi, which is approximately 50% percent of the cracking stress of the concrete (1.1 ksi). After applying the magnification factor, the maximum single lane loaded stress at midspan was 736 psi tension.

Figure 3.16 shows the maximum tensile strain in the girder bottom flange at midspan for the static Load Cases 1 through 5 during Test 2. The maximum midspan flexural strain measured during Test 2 (65.2 microstrain tension) occurred in the bottom flange of girder 3 for Load Case 5. The corresponding maximum tensile stress in the girder bottom flange (assuming E_c=7820 ksi) was 510 psi, which is less than 50% percent of the cracking stress of the girders (1.1 ksi). After applying the magnification factor of 1.39, the maximum single lane loaded stress at midspan is 709 psi tension.

By comparing Load Case 1 with Load Case 5 and Load Case 2 with Load Case 3, the transverse symmetry of the bridge and loading can be seen. Also, note that the computed design live load stress from an HS20-44 truck was calculated to be 2.04 ksi and 2.41 ksi tension for the interior and exterior beams, respectively. The above results demonstrate a fairly conservative design for the UHPC bridge.

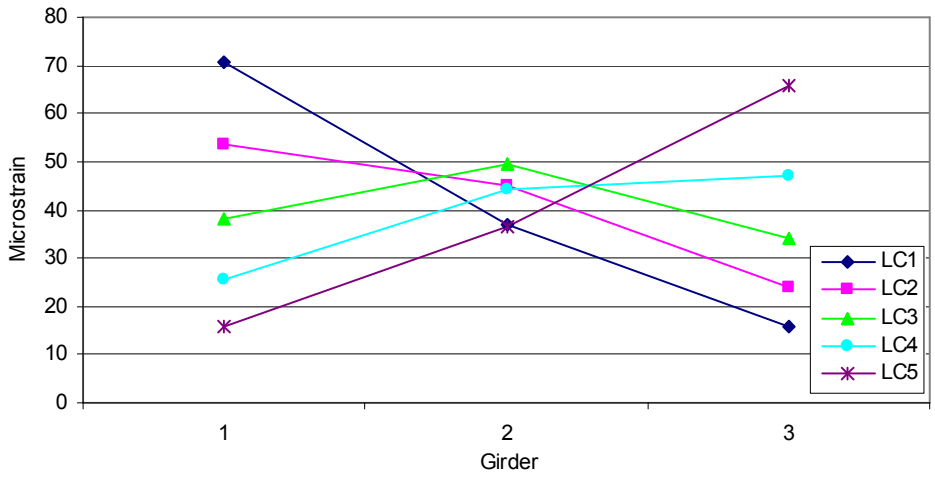

Figure 3.15. Maximum bottom flange girder strains at midspan for Test 1.

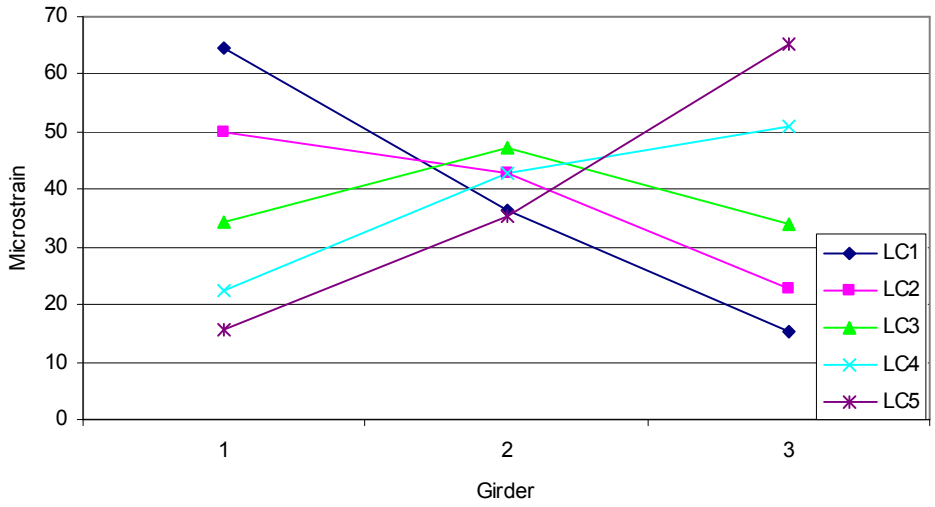

Figure 3.16. Maximum bottom flange girder strains at midspan for Test 2.

3.7.2. Neutral Axis

The neutral axis location of each girder was determined by using the top and bottom flange strains to interpolate the location where the strain in the girder is zero. If the girder is acting separately from the concrete deck, the structure is considered non-composite.

However, partial and full composite action is generated when the girder and concrete deck act together to some degree. Generally the neutral axis location will be located higher (towards the top flange) as the degree of composite action increases.

Table 3.4 summarizes the location of the neutral axis calculated for the interior and exterior girders during Test 1 and Test 2. In addition, the theoretical composite interior and exterior girder neutral axes are presented as design. The neutral axis of the interior girder correlates fairly well with the theoretical composite interior girder location of 30.09 in for both Test 1 and Test 2. During Test 1, the interior girder neutral axis ranged from 27.7 in. for Load Case 1 to 34.3 in. for Load Case 4. The interior girder neutral axis in Test 2 ranged in values from 27.4 in. for Load Case 1 to 33.1 in. for Load Case 3.

The neutral axes of the exterior girders are considerably higher than that of the theoretical exterior girder neutral axis location of 24.92 in. for all load cases during both load tests. During Test 1, the exterior girders neutral axes ranged in values from 27.8 in. for Load Case 1 and Load Case 5 to a maximum of 35.6 in. in girder 3 during Load Case 5. The exterior girders neutral axes in Test 2 ranged in values from 27.8 in. for girder 1 for Load Cases 5 to a maximum of 36.1 in. for girder 3 for Load Case 5. The neutral axes calculated confirm the composite action behavior of the UHPC bridge and suggests a larger effective flange width than used in the calculations of the theoretical composite neutral axes.

Table 3.4. Neutral axis location measured from the bottom flange.

	Interior Girder Range (in.)	Exterior Girder Range (in.)
Test 1	27.7 - 34.3	27.8 - 35.6
Test 2	27.4 - 33.1	27.8 - 36.1
Design	30.09	24.92

3.7.3. Load Fraction

Approximate load fractions were calculated from the measured strains at midspan. Lateral load fractions were approximated from Equation 3.1 using test data from the bridge.

$$LF_i = \frac{\varepsilon_i}{\sum_{i=1}^{n} \varepsilon_i} \quad \text{load fraction} \tag{3.1}$$

Where: LF_i = load fraction of the ith girder (lanes/girder)

ε_i = strain of the ith girder

$\sum \varepsilon_i$ = sum of girder strains

n = number of girders

A summary of the maximum load fractions for each load case is shown in Figure 3.17 and Figure 3.18 for Test 1 and Test 2, respectively. The graphs of the load fractions correlate well with the transverse position of the test trucks. The percentage of load carried by a girder decreases as load is positioned farther away. In addition, the symmetrical behavior of the bridge is again evident by comparing Load Case 1 with Load Case 5 and Load Case 2 with Load Case 4. The load fractions calculated here are used in the following results to determine experimental distribution factors.

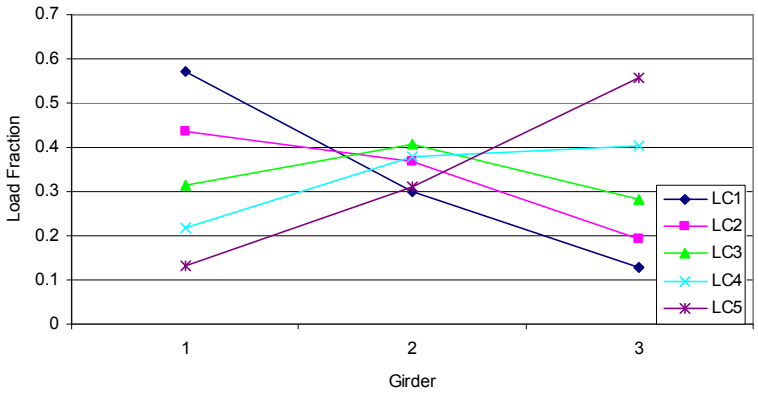

Figure 3.17. Experimental load fractions from Test 1.

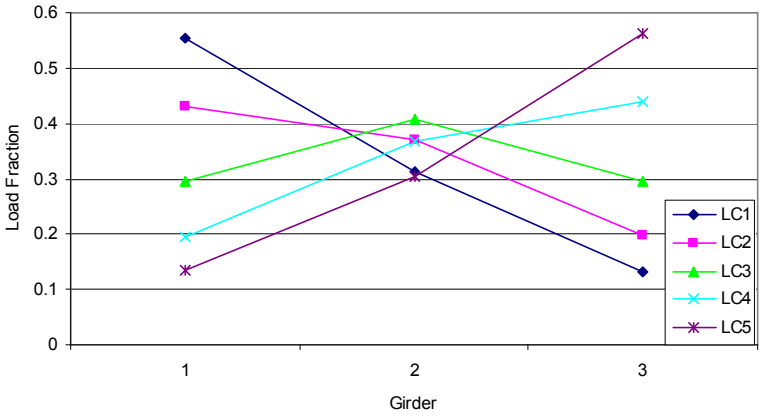

Figure 3.18. Experimental load fractions from Test 2.

3.7.4. Distribution Factors

Experimental distribution factors were calculated from the previous load fractions. Distribution factors were determined by superimposing the load fractions from two single lane load cases. The load distribution factors were compared to bridge design code distribution factors [4]. The maximum distribution factors and the design distribution factors are shown in Figure 3.19 for Test 1 and Test 2. Bridge design code distribution factor for two lanes loaded is labeled as "Design" and the corresponding load cases are labeled such that "LC1 + LC5" is the effective result of superimposing Load Case 1 and Load Case 5.

The experimental distribution factors are all less than the AASHTO [4] factors. The maximum experimental distribution factor for the exterior girders was 0.79 which occurred during Test 1 in girder 1 by superimposing Load Case 1 and Load Case 4. The maximum interior experimental distribution factor was 0.68 which occurred by superimposing Load Case 1 and Load Case 4 and also Load Case 2 and Load Case 5. Due to the experimental distribution factors all being less, the AASHTO distribution factors used for the design of the

UHPC bridge are shown to be slightly conservative. It can also be seen in Figure 3.19 that the experimental distribution factors are symmetrical.

In general, there is a good correlation between Test 1 and Test 2. However, there is a slight variation in the exterior girders which could be attributed to a difference in the transverse location of the truck for each test. In addition, the gravel may not have been evenly distributed in the dump truck which could cause an uneven wheel line load. The higher values for girder 1 and lower values for girder 3 in Test 1 could be a result of the load distributed slightly heavier towards the girder 1 side of the truck.

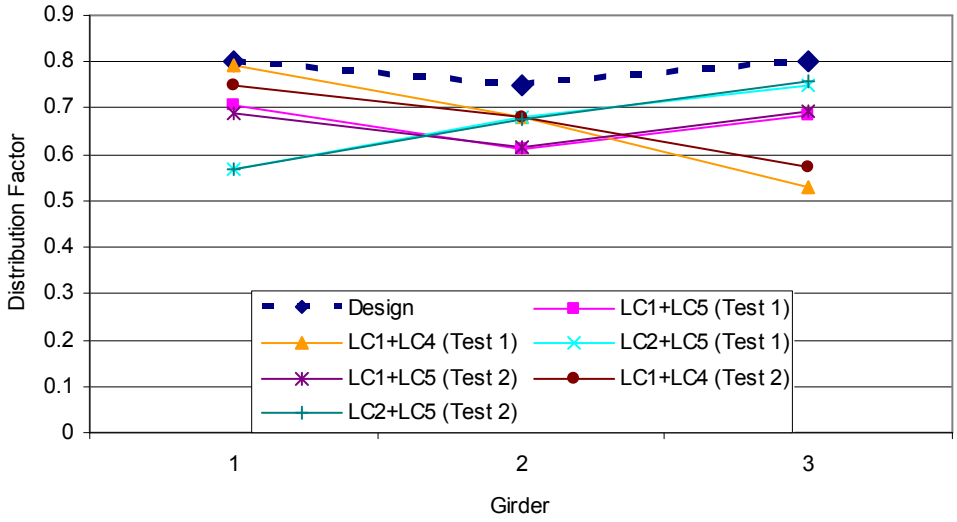

Figure 3.19. Experimental and AASHTO distribution factors from Test 1 and Test 2.

3.7.5. Dynamic Results

Dynamic test were performed on the UHPC bridge as previously mentioned. However, the actual transverse position of the truck for Load Case 6 and Load Case 7 were not at 2 ft from curb due to the speeds at which the truck was traveling. The estimated

distance from curb was 3.5 ft. and 4 ft for Load Case 6 and Load Case 7, respectively. The recorded speeds the truck was traveling were within 1 mph of the target speed for every load case. It is also noted that there was a significant bump at the interface of the gravel roadway and the bridge deck. This may have created notable truck dynamics.

Figure 3.20 shows the time history plot for strain of the three girders (labeled 1, 2, 3) at midspan during Load Case 7 in Test 1 which induced the largest strain in a single girder. The maximum strain occurred in girder 1 with a value of 103.5 microstrain tension. After applying the magnification factor, the associated stress is 1076 psi tension, slightly less than the cracking stress of 1.1 ksi but still well below the design stress of 2.41 ksi.

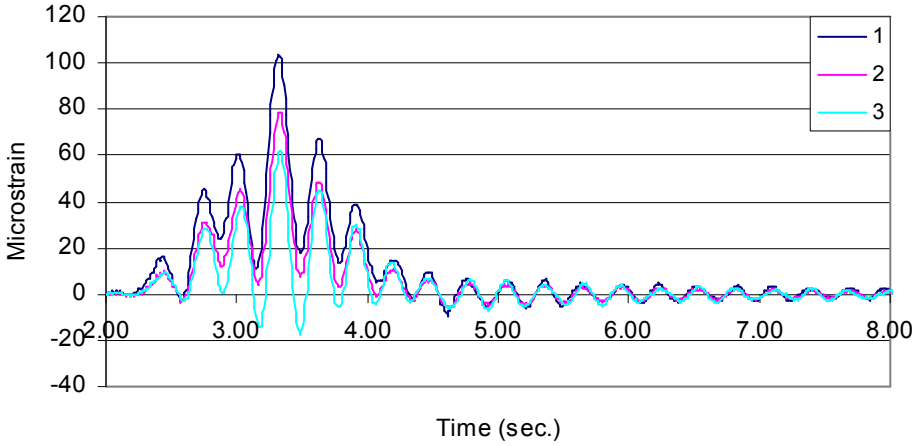

Figure 3.20. Bottom flange midspan girder strain versus time, Load Case 7, Test 1.

The period and frequency calculated from Test 1 for both the interior and exterior girders are T_d=0.292 sec. and ω_d=21.5 rad./sec., respectively. The damping ratios are ζ=0.016 for girder 1 and ζ =0.017 for girders 2 and 3. The damping ratios are less than the assumed equivalent viscous damping ratio of 2% given by AASHTO [4] for concrete construction. The differences here are insignificant and are most likely a result of the UHPC

having a significantly higher strength than typical concrete. The dynamic amplification ratios for Test 1 computed by comparing maximum strains from Load Case 9 and Load Case 3 are 1.80, 1.53, and 1.82 for girders 1, 2, and 3, respectively. Load Case 9 was chosen since the transverse position for the dynamic and static load cases correlated. The three dynamic amplification ratios are higher than the 1.33 factor recommended by AASHTO [4].

The dynamic load cases in Test 2 varied slightly from Test 1. Due to the large bump which was experienced in Test 1, the position of Load Case 6 and Load Case 7 were moved to the other side (east side) of the bridge during Test 2. The targeted location was 2 ft from the curb; however, as in Test 1, the estimated distance from curb was 3.5 ft and 4 ft for Load Case 6 and Load Case 7. In addition, the speeds reached in Load Case 7 and Load Case 9 were 5 mph less (i.e., 30 mph) than the target speed of 35 mph.

The maximum strain during Test 2 occurred in girder 3 at a strain of 71.9 microstrain tension. After applying the magnification factor, the associated stress is 781.5 psi tension. The period and frequency computed from Test 2 for all the girders are T_d=0.291 sec. and ω_d=21.6 rad./sec. respectively. The damping ratios are ζ=0.016 for each girder. Similar to the first test, the damping ratios are comparable to the recommended AASHTO [4] damping ratio of 2% for concrete structures. Again, the differences here are inconsequential and are assumed to be a result of the concrete strength. The dynamic amplification ratios computed by comparing maximum strains from Load Case 9 and Load Case 3 are 1.35, 1.07, and 1.23 for girders 1, 2, and 3, respectively. Except for girder 1, the dynamic amplification ratios are less than the dynamic factor of 1.33 recommended by AASHTO [4]. Load Case 9 was chosen since the transverse position for the dynamic and static load cases correlated. The dynamic effects from Test 2 appear to be lower than Test 1 because the weight of the vehicle

for Test 2 was less (4.1% difference) than Test 1 and the speed reached in Test 2 was 5 mph less than Test 1. Also, the dynamic effects from Test 1 may be higher because the truck was bouncing significantly due to the bump at the bridge approach.

3.8. COMPARATIVE RESULTS

3.8.1. Bottom Flange Midspan Girder Strain Comparisons

The strain values for Test 1 are slightly greater than Test 2 in all cases; however, the shape of the curves for Test 1 and Test 2 are similar to one another. These results were expected since the weight of the truck for Test 1 was 4.1% greater than the weight of the truck for Test 2. Figure 3.21 presents a graph of the maximum bottom flange girder strain at midspan for both Test 1 and Test 2 for the load cases and the values for Test 2 are increased by 4.1%. As can been seen in Figure 3.21, the maximum girder strains from Test 1 are nearly identical to the strains from Test 2 after being adjusted.

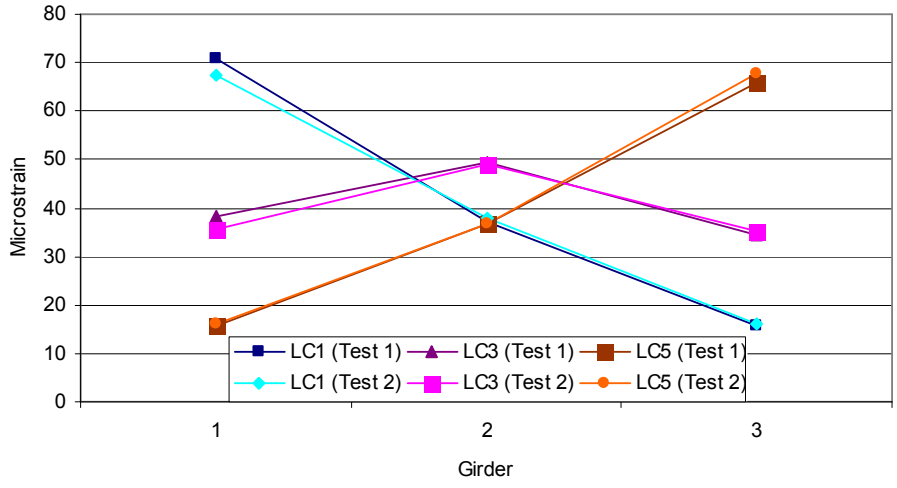

Figure 3.21. Bottom flange girder strains at midspan from Test 1 and Test 2.

Overall, Test 1 and Test 2 produced consistent results. The higher strain values obtained in Test 1 were accounted for due to the difference in the weights of the trucks. Other dissimilarities could possibly be attributed to differences in truck placement, truck orientation, and transducer location.

3.8.2. Comparison of Live Load Tests and Laboratory Tests

Assuming stresses and strains remain linear up to the point of cracking, the girder strains from the live load tests can be compared to the flexural testing of the large-scale laboratory test. Using the calculated prestressing force in the large-scale beam (1517 kips) and the longitudinal bottom flange stress at centerline, the prestressed state of the bottom flange of the large-scale beam can be determined. The large-scale beam had a prestressed state of 5.81 ksi compression (743 microstrain) at the bottom surface of the concrete. The self-weight of the large-scale beam had an affect of 0.58 ksi tension at the bottom surface resulting in a final stress of 5.23 ksi compression (669 microstrain) before any additional loading. Subtracting the strain value at which non-linearity occurred during the large-scale flexure testing, the resultant cracking stain level can be calculated as 80 microstrain tension or 0.63 ksi, which is significantly lower than the assumed 1.1 ksi cracking stress in tension.

Similarly the prestressed state of the bottom concrete surface of the bridge beams can be determined. The concrete stress level at the bottom surface due to prestressing and dead load for the interior bridge beam is 1.10 ksi compression (140 microstrain) and for the exterior beams is 1.89 ksi compression (241 microstrain).

The maximum pseudo-static bottom flange concrete strains measured at the midspan during the live load field testing were 49 microstrain and 71 microstrain tension for the

interior and exterior girders, respectively. The resulting strain due to prestressing, dead load, and live load at the bottom surface is 91 microstrain compression for the interior girder and 170 microstrain compression for the exterior girders.

Using the experimental cracking strain obtained above (80 microstrain tension), the interior girder has the capacity for 171 microstrain tension or 1.34 ksi in addition to the live load level before reaching the cracking service level limit state, and the exterior girder has the capacity for an additional 250 microstrain tension or 1.96 ksi. Even at the maximum measured dynamic strain of 103.5 microstrain tension, which occurred at the exterior girder in Test 1, the exterior girder has an additional strain capacity of 217.5 microstrain or 1.70 ksi tension.

3.9. CONCLUSIONS

The background, design, construction, and test results of the first UHPC bridge built in the United States were discussed in this paper. Based on the results of the large-scale laboratory flexure test and live load field tests, the following conclusions are made:

1. The large-scale flexure test results correlated well with the analytical model using the strain compatibility approach and, furthermore, the test results verified that the service level and ultimate level flexural capacities are adequate for the Wapello County bridge. The calculated service moment capacity of the bridge beam was determined experimentally to be 4,760 ft-kips which is greater than the applied service bridge moment of 4,624 ft-kips. The calculated ultimate moment capacity of the bridge beam was determined analytically to be 7,620 ft-kip which is greater than the applied ultimate bridge moment of 7,350 ft-kip.

2. The maximum design live load stresses at midspan due to an HS-20 truck for the interior and exterior girders were calculated to be 2.04 ksi and 2.41 ksi tension, respectively. After applying the magnification factors, the maximum static girder stress at midspan was 736 psi tension and the maximum dynamic girder stress was 1,076 psi tension. All stresses were well below the expected live load stresses and the cracking stress of UHPC (1.1 ksi). No cracks were observed in the UHCP girders or concrete deck.
3. The girder neutral axes were generally at or above the theoretical composite neutral axes, confirming composite action between the girders and bridge deck.
4. The experimental distribution factors correlated well with design distribution factors. In all cases, the experimental distribution factors were less than the design distribution factors which suggests a slightly conservative design.
5. The dynamic results from Test 1 indicated a slightly exaggerated amplification; however, dynamic results from second live load test compared well with AASHTO design recommendations.
6. Overall, the results from the two live load tests were similar and the UHPC bridge performed as expected under the load conditions.

Research has shown that UHPC has superior material characteristics compared to other types of concrete. Both its tensile and compressive strengths are much higher than conventional concrete. The construction of this bridge demonstrates the ability of UHPC to be used as an alternative material for bridge design. The live load field testing further validates the performance of UHPC. Future monitoring and cost analysis of the UHPC bridge would confirm the durability and lifespan while determining the overall expense of

constructing and maintaining the bridge. Any additional tests would also expand the UHPC system data base and further validate and calibrate design procedures.

3.10. REFERENCES

1. T. Wipf, B. Phares, S. Sritharan, B. Degen, and M. Giesmann. *Design and Evaluation of a Single-span Bridge Using Ultra-High Performance Concrete.* Report to the Iowa Department of Transportation. 2008.
2. B. Graybeal and J. Hartmann. *Strength and Durability of Ultra-High Performance Concrete*. Report to the 2003 Concrete Bridge Conference, 2003.
3. B. Degen. *Shear design and behavior of Ultra-High Performance Concrete.* Iowa State University, 2006.
4. American Association of State Highway and Transportation Officials (AASHTO), *AASHTO LRFD Bridge Design Specifications, 1998*. American Association of State Highway and Transportation Officials, Washington, D.C.

CHAPTER 4. GENERAL CONCLUSION

This thesis summarized two separate papers related to the performance evaluation and demonstration of two bridges in the state of Iowa that make use of innovative materials and bridge design.

Chapter 2 presented the design and live load field test results of a bridge that has employed a concrete steel-free deck (SFD) system. In the summer of 2004, the first bridge in the United States to use the SFD system was constructed in Tama County, Iowa. The SFD system utilizes a fiber reinforced concrete deck that is laterally restrained by attaching steel straps to the top flanges of the supporting girders. Internal arching action is developed within the concrete to resist load by preventing the outward lateral displacement of the supporting girders. By removing the steel reinforcement within the concrete, the life expectancy and durability of the bridge deck is expected to improve significantly by eliminating the corrosion of the steel.

Live load field testing was performed on the Tama County bridge soon after the completion and approximately one year of service. Based off the results of the live load testing, there is no indication of a reduction in structural performance due to the design of the deck at service level. Continued monitoring and evaluation of the Tama County bridge will verify the life expectancy and durability of the SFD system. The Tama County bridge performed well during the live load testing and should be recommended as an alternative design to the conventional steel reinforced concrete deck.

Chapter 3 presented the design and live load field test results of a bridge that has utilized a newly developed material called Ultra-High Performance Concrete. In the fall of

2005, the first bridge in the United States to implement UHPC was constructed in Wapello County, Iowa. UHPC is a high performance material that can achieve compressive strengths of up to 30,000 psi and tensile strengths of approximately 1,700 psi. The high strengths make UHPC a desirable material for structural applications by reducing section sizes and increasing span lengths. Also, UHPC is a highly dense material making it impermeable to water and chlorides, thus protecting steel reinforcement from corroding.

Live load testing was performed on the Wapello County bridge soon after the completion of the bridge and approximately after one year of service. The live load testing confirmed the superior structural performance of UHPC. The Wapello County bridge performed within the design service level limits under the loading conditions and a developed dynamic model also verified the results. Based off the live load test results, UHPC should be recommended as an alternative material to be used in future bridge applications. Future monitoring and cost analysis of the UHPC bridge would confirm the durability and lifespan while determining the overall expense of constructing and maintaining the bridge.

Investigations and demonstrations of projects similar to these are vital to the acceptance and implementation of innovative materials and bridge designs. The results of this thesis and any future related research will expand the data base and application as well as further calibrate the design procedures and use of the innovative materials presented here.